Pergamon

PII S0016-7037(01)00817-1

Burial of redox-sensitive metals and organic matter in the equatorial Indian Ocean linked to precession

DELPHINE PAILLER,[1] EDOUARD BARD,[1,*] FRAUKE ROSTEK,[1] YAN ZHENG,[2] RICHARD MORTLOCK,[2] and ALEXANDER VAN GEEN[2]

[1]CEREGE, Universite Aix-Marseille III and CNRS, UMR-6635, Europole de l'Arbois, BP 80, 13545 Aix-en-Provence cedex 4, France
[2]Lamont-Doherty Earth Observatory of Columbia University, Palisades, NY 10964, USA

Abstract—Authigenic metals (uranium, cadmium, and molybdenum), organic carbon (OC) and total C_{37} alkenone (totC_{37}) concentrations were measured for the last 350 kyr in core MD900963, located in the eastern equatorial Arabian Sea. Authigenic metal concentrations on a carbonate-free basis range between 1 and 17 ppm, 0.5 and 6 ppm, and 0.5 and 4 ppm for U, Cd, and Mo, respectively. The profiles are characterized by well-defined 23 kyr cycles between oxic and mildly suboxic conditions. The redox-sensitive metal profiles also follow variations in the concentrations of OC (0.2–0.9%) and alkenones (0.2–6.7 ppm). The coupled variations in inorganic and organic constituents are attributed to a 23-kyr cycle in primary production above site MD900963, as suggested by clear correlations with independent micropaleontologic proxies (primary productivity indices based on foraminifera and coccoliths and fragmentation of foraminiferal shells). The 23-kyr cycles do appear to be primarily driven by productivity rather than changes in bottom water oxygen. Comparison with other records indicates that if this interpretation is correct, productivity variations across much of the Indian Ocean have been dominated by precessional forcing, with high productivity in phase with low summer insolation in the Northern Hemisphere. This interpretation contrasts with the traditional attribution of enhanced productivity in the Indian Ocean with periods of high summer insolation. *Copyright © 2002 Elsevier Science Ltd*

1. INTRODUCTION

The Arabian Sea is an area of very high productivity driven by the Asian monsoon, a pronounced climate feature of global significance (Nair et al., 1989; Brock et al., 1991; Curry et al., 1992; Haake et al., 1996). Since these conditions are reflected in the nature of sediment accumulating on the seafloor, it is not surprising that sediment cores from the Arabian Sea have long been studied to reconstruct past variations in the Asian monsoon in response to orbital changes in insolation. Proxy records from various locations have traditionally been used to infer a connection between enhanced productivity in the Arabian Sea and summer insolation over Asia (Prell, 1984; Clemens and Prell, 1990; Clemens et al., 1991, 1996; Murray and Prell, 1992; Emeis et al., 1995). In contrast, Reichart et al. (1997), Rostek et al. (1997), and Schubert et al. (1998) have shown across several glacial-interglacial cycles that the accumulation of organic carbon in the northeast Arabian Sea was strongly dominated by a 23-kyr cycle, with maxima in organic carbon content corresponding to periods of low summer insolation in the Northern Hemisphere. Despite these extensive efforts, a consensus has yet to emerge on the basic nature of climate processes recorded by a series of well-dated sediment records from the region. We contribute to the debate in this paper by (1) presenting new downcore records for the redox-sensitive metals Cd, Mo, and U at a site near the Maldives in the southeastern Arabian Sea, (2) interpreting these records in the context of a broader set of measurements performed on the same core (organic carbon, alkenone concentration, primary productivity indices based on foraminifera and coccoliths, and fragmenta-

tion of foraminiferal shells), and (3) pointing out strikingly related features in several sediment cores distributed throughout the Indian Ocean.

During the SEYMAMA expedition of the R.V. *Marion Dufresne* in 1990, core MD900963 was recovered from the eastern slope of the Maldives archipelago at 5°03′N and 73°53′E at a water depth of 2446 m (Fig. 1). Compared to the western Arabian Sea, summer winds at the core site are weaker (6–10 m/s compared to 12–15 m/s), more westerly, and not oriented in a direction relative to the coast that favors upwelling. This wind pattern is well established from May to September and extends to October closer to the equator (Knox, 1987; Naidu et al., 1992, 1999). Satellite-based pigment distributions suggest that primary production (PP) in the Maldives is ~160 gC/m^2/yr (Antoine et al., 1996), considerably less than in the northwestern Arabian Sea of 200 to 600 gC/m^2/yr (Antoine et al., 1996). Elevated pigment concentrations occur mainly from August to October (Antoine et al., 1996) and probably reflect upwelling along the west coast of India (Sastry and D'Souza, 1972; Sharma, 1978). Local wind stress may play a role as well (Naidu et al., 1999).

The water column is relatively well oxygenated at the core site today. Dissolved oxygen concentrations reach a minimum of 40 to 60 μmol/L between 200 and 800 m depth before increasing steadily to 150 μmol/L at the bottom depth of ~2500 m (Levitus and Boyer, 1994a). The core site is influenced by three principal water masses. A hydrological front separates two water masses above 2000 to 2500 m depth across the Indian Ocean at ~10°S (Wyrtki, 1973; Tchernia, 1980). To the north, warm and highly saline surface water sinks and mixes with the Red Sea and Persian Gulf outflows to form oxygen-depleted north Indian high salinity intermediate water (NIHSIW): S‰ > 34.8‰ (Tchernia, 1980; Olson et al., 1993).

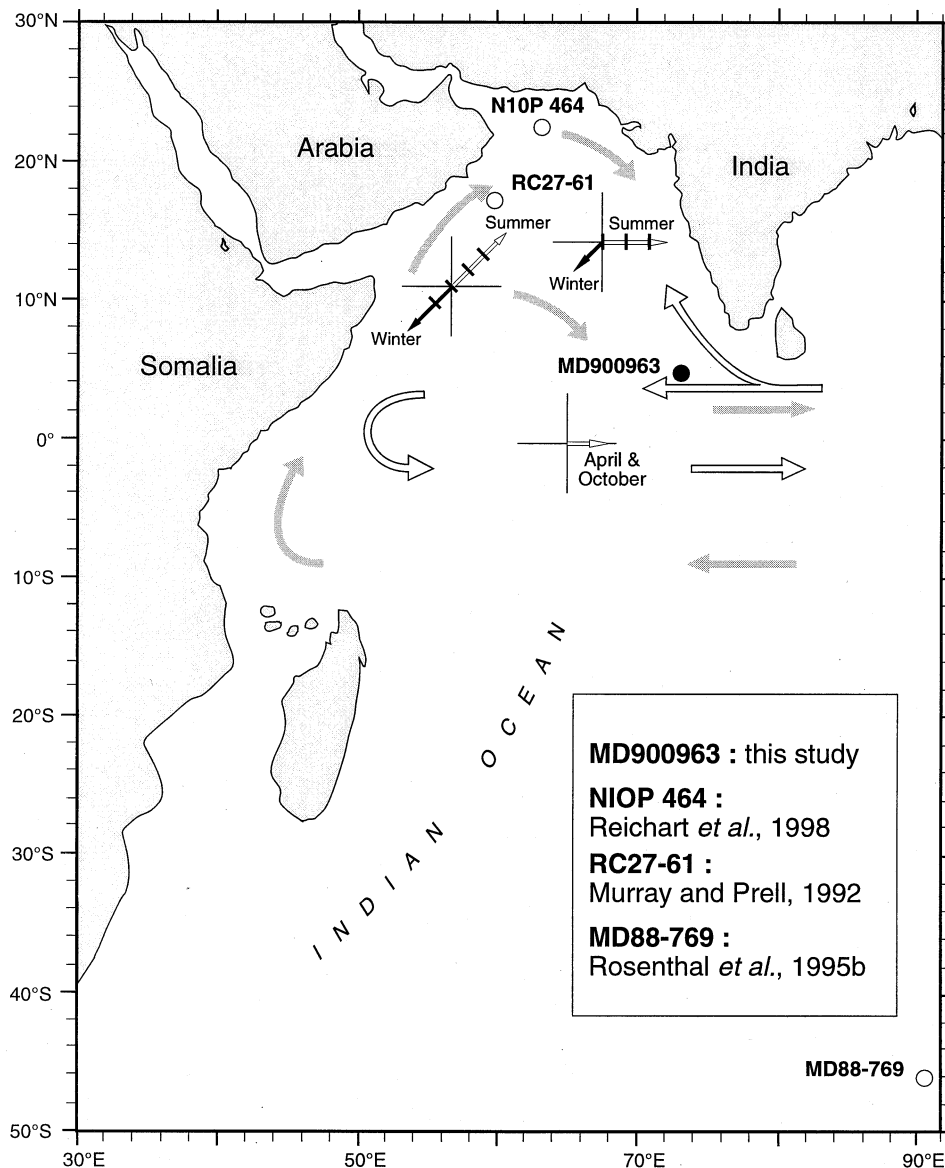* Author to whom correspondence should be addressed (bard@cerege.fr).

Fig. 1. Core MD900963 location and modern climatology of the Arabian Sea. Full gray arrows are for summer sea surface circulation, empty arrows stand for winter sea surface circulation (adapted from Wyrtki, 1973). Wind roses display seasonal tendencies for wind strength (one graduation on the arrows represents ~5 m/s) and direction (Da Silva et al., 1994). Open dots also show the locations of cores used in the discussion: RC27-61 (Murray and Prell, 1992), MD88-769 (Rosenthal et al., 1995b), NIOP 464 (Reichart et al., 1998).

To the south, cold, relatively fresh (S‰ < 34.7‰) and well-oxygenated surface water from the polar front sinks below subtropical gyre surface water between 45°S and 60°S. Antarctic intermediate water (AAIW) extends northward between 700 and 2000 m before losing its properties by mixing with NIHSIW of the same density in the vicinity of the front at 10°S (Wyrtki, 1973; Tchernia, 1980). Below 2000 to 2500 m, the deep Indian Ocean is occupied by a rather uniform water mass (34.7 < S‰ < 34.8) of circumpolar and Atlantic origin, spreading northward into the Indian Basin (Wyrtki, 1973; Mantyla and Reid, 1995). With temperature and salinity of 2°C and 34.75‰ (Levitus et al., 1994; Levitus and Boyer, 1994b), the site of core MD900963 lies within the upper part of the Indian

Ocean deep water and potentially, therefore, could also be influenced by changes in NHISIW. The oxygen content (150 μmol/L) is lower than in the deep Antarctic (200–220 μmol/L) (Levitus and Boyer, 1994a), reflecting oxygen utilization during the northward transit of deep Antarctic circumpolar water (Stuiver et al., 1983; Kroopnick, 1985).

Oxygen stable-isotope measurements of planktonic foraminifera *Globigerinoides ruber* (white) provide a detailed chronological framework for the core (Fig. 2a) Bassinot et al., 1994a). An orbitally-derived age model was develop by tuning the $\delta^{18}O$ record to the ice-volume model of Imbrie and Imbrie (1980). The upper 19 m of the core provides a continuous record of the past 350 kyr at a sedimentation rate of 5.6 ± 1.4
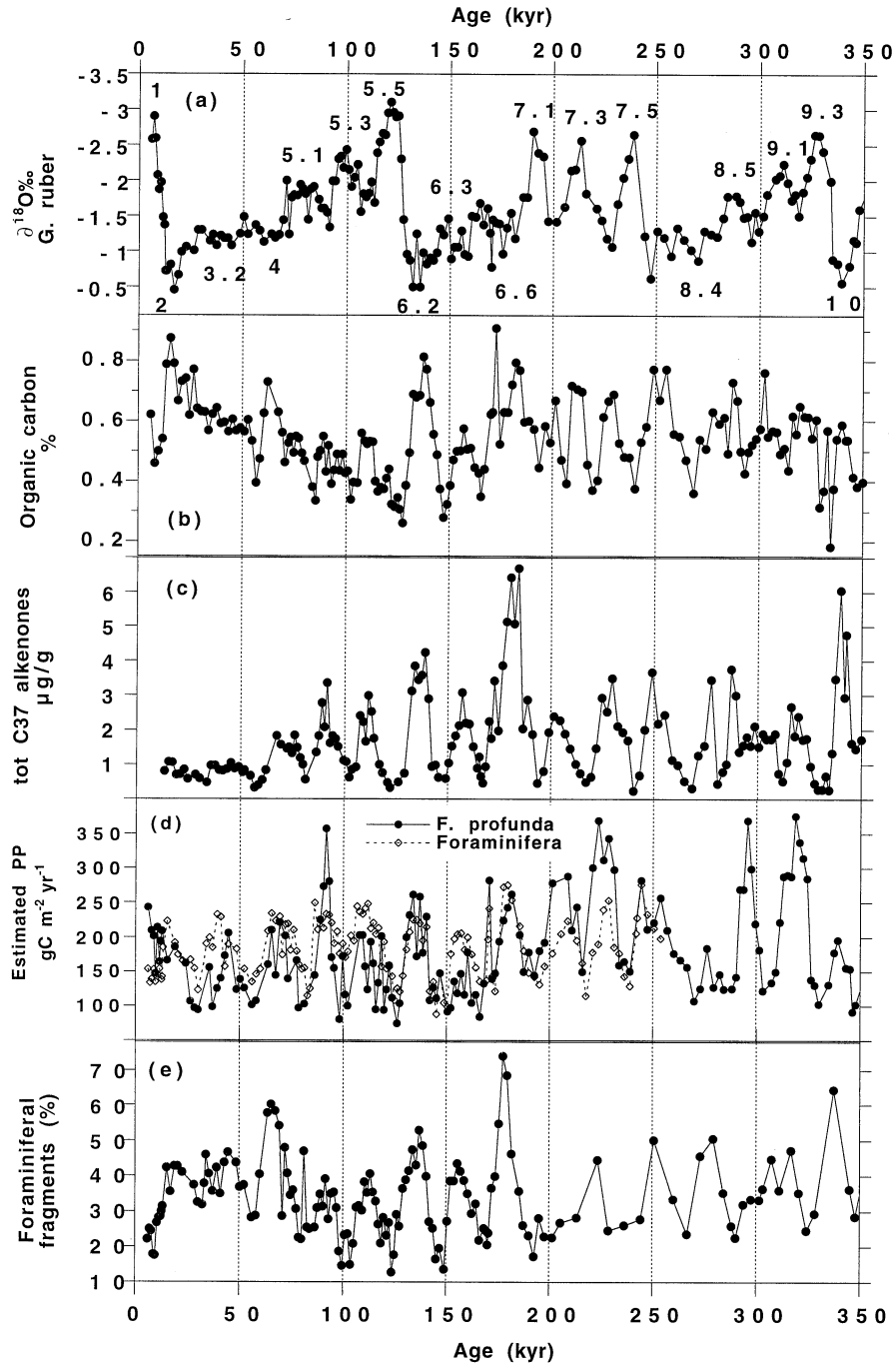
Fig. 2. Biogenic indices for the last 350 kyr in core MD900963: (a) $\delta^{18}O$ stratigraphy from Bassinot et al. (1994b); (b) OC content; (c) C_{37} alkenones concentration; (d) PP estimates obtained from *F. profunda* (Beaufort et al., 1997) and planktonic foraminifera (Cayre et al., 1999), this latter being limited to the last 270 kyr; (e) fragmentation index of shells of foraminifer expressed as the percentage of the sum of whole foraminifers plus fragments to whole foraminifers (Bassinot 1994a). Data for OC content and totC$_{37}$ are listed in Table 3.

cm/kyr. Because of the relatively constant sedimentation rate, concentration profiles of the constituents in this core closely resemble profiles of mass-accumulation rates (Rostek et al., 1997). The carbonate content of core MD900963 varies between 40 and 80% (Bassinot et al., 1994b). The power spectra of the carbonate content of the core, which is its major constituent, is dominated by different major frequencies (Bassinot et al., 1994b) than the organic carbon (OC) concentration for the top 10 m (Rostek et al., 1997). This indicates that downcore variations in the concentration of noncarbonate constituents reflect changes in input rather than variations in dilution (Rostek et al., 1997). The age model is consistent with an indepen-

Table 1. Detection limits, accuracy, and reproducibility of the analyses.

	Detection Limits		Standard Sediment					
	This study	Zheng et al. 2001c	This study			Zheng et al. 2001c		
element	ppm	ppm	ppm	RSD (%)	n	ppm	RSD (%)	n
Mo	0.03	0.06	2.58 ± 0.10	3.80	11	2.57 ± 0.11	4.2	15
Cd	0.04	0.08	1.10 ± 0.04	3.2	11	1.12 ± 0.05	4.5	7
U	0.05	0.03	4.34 ± 0.12	2.7	11	4.64 ± 0.05	1.1	15
Th	0.07	0.06	10.07 ± 0.44	4.4	9	10.61 ± 0.46	4.3	15

dent stratigraphic marker at 3.5-m depth, an interval rich in volcanic shards and low in carbonate (Bassinot, 1993). The $\delta^{18}O$-derived age of 71 ka is consistent with a radiometric age of 73 ± 4 ka (Chesner et al., 1991) for volcanic ash from the well-documented Toba eruption in Sumatra (Ninkovich et al., 1978; Westgate et al., 1998). Previous paleoceanographic proxies measured at high resolution in core MD900963 include the degree of fragmentation of foraminifera (Bassinot et al., 1994a), the flux and concentration of OC and alkenones (Rostek et al., 1997), and faunal studies of coccoliths (Beaufort et al., 1997) and planktonic foraminifera (Cayre et al., 1999).

The present contribution includes detailed downcore records of concentrations of the redox-sensitive metals uranium (U), cadmium (Cd), and molybdenum (Mo) over the past 330 kyr, in comparison with an extension of the organic carbon and alkenone record between 170 and 350 ka (10–19 m core depth).

Long-chain C_{37}-alkenones are produced by a few species of the class Prymnesiophyceae (Volkman et al., 1980a,b; Marlowe et al., 1984). The concentration of alkenones, therefore, provides a qualitative measure of productivity by these organisms, in contrast to bulk organic carbon, which is less specific (Prahl and Muelhausen, 1989; Rostek et al., 1997; Schubert et al., 1998; Villanueva et al., 1998).

Concentrations of U, Cd, and Mo are also influenced by primary production, because the degradation of organic matter reaching the sediment consumes a sequence of oxidants, i.e., oxygen, nitrate, iron (Fe), and manganese (Mn) oxides and sulfate (Froelich et al., 1979; Berner, 1981). Different threshold levels of oxidant consumption trigger a series of reactions that lead to precipitation of U, Cd, and Mo in the sediment (Lapp and Balzer, 1993; Legeleux et al., 1994; van Geen et al., 1995; Rosenthal et al., 1995a,b; Crusius et al., 1996; Zheng, et al., 2000, 2001a). Authigenic U precipitation typically starts at the redox potential of Fe-oxide reduction (Cochran et al., 1986; Klinkhammer and Palmer 1991; Zheng, et al., 2001a). The threshold level for authigenic Cd formation is reached next under increasingly reducing conditions and appears to require nanomolar levels of hydrogen sulfide (Rosenthal et al., 1995a; van Geen et al., 1995; Kuwabara et al., 1999). Mo enrichments in marine sediments are largely limited to anoxic sediments (Crusius et al., 1996; Zheng et al., 2000), although suboxic conditions can also cause Mo enrichment in association with the precipitation of Mn oxides (Shimmield and Price, 1986). There is an additional link between productivity and authigenic metal accumulation in the sediment reflecting the U and Cd fraction associated with settling biologic matter (Anderson, 1987; van Geen et al., 1995; Zheng et al., 2001a). However,

this fraction contributes to only ~10% of the total authigenic U in marine sediment if the bottom water dissolved oxygen concentration is ~140 μmol/L (Zheng et al., 2001a).

2. ANALYTICAL METHODS

2.1. Authigenic Metals

The core was sampled every 10 cm ($\approx$2 kyr) in plastic vials to measure Mo, Cd, U, and Th by isotope dilution and inductively-coupled plasma mass spectrometry (ICP-MS). Dried and ground sediment weighing ~10 mg was spiked with ^{95}Mo, ^{111}Cd, and ^{236}U. Ultrapure (Seastar) concentrated $HClO_4$, HF, and HNO_3 was successively added on a hotplate until complete digestion and final redissolution in 1% HNO_3, following the method of Zheng et al. (2001c). The solution was analyzed with a VG PlasmaQuad II+ ICP-MS at LDEO under standard recommended conditions. Detection limits and precision of the method were monitored during the entire process by repeated analysis of spiked blanks, an internal laboratory sediment standard (MC-E Pb6, Santa Barbara Basin), and several replicates of the studied samples. Mo, Cd, U, and Th determinations were reproducible to 3 to 4.5%, and results for standard sediment material were in agreement with previously reported values (Table 1). Isobaric interferences were checked for Mo and Cd by measuring three different unspiked samples. The $^{111}Cd/^{113}Cd$ ratio of the unspiked samples (1.00) was close to the true ratio (1.04) within the precision of the method. On the other hand, $^{95}Mo/^{98}Mo$ ratios for the unspiked samples (0.74–0.85) were significantly above the natural ratio (0.6611), indicating an interference at ^{95}Mo. Overestimation of natural ^{95}Mo was negligible compared to the ^{95}Mo spike added, however.

2.2. Organic Carbon and Alkenones

OC was determined by gas chromatography with a method adapted from Verardo et al. (1990). Carbonate carbon was removed by in situ acidification with sulfurous acid inside aluminum sample cups. Precision of analysis with a Fisons NA-1500 Elemental Analyzer (Carlo Erba NA-1500 Elemental Analyzer) was on the order of 5%.

Alkenones were extracted and quantified by the manual procedure used at CEREGE for the 0- to 350-kyr interval in the same core (Sonzogni et al., 1997). Briefly, 1 to 2 g of ground dry sediment was extracted with a mixture of CH_2Cl_2:CH_3OH (2:1, 2 $\times$ 20 mL) and CH_2Cl_2 (1 $\times$ 20 mL). After concentration, the total extract was analyzed with a gas chromatograph fitted with an on-column injector and flame ionization detector with an estimated precision of 15%. The concentration of total C_{37} alkenones (totC_{37}) was normalized to a n-C_{36} internal standard added to each sample before the extraction. Precision and accuracy of our protocol was checked in the framework of the international alkenone intercomparison (Rosell-Melé et al., 2001).

3. RESULTS

3.1. Authigenic Metals

Total metal concentrations are listed in Table 2. These concentrations were also converted in concentrations on a carbon-

Table 2. Concentrations of total U, cfb total U, Uauth, cfb Uauth, Th, cfb Th, Mo, cfb Mo, Cd and cfb Cd for core MD900963.

Depth cm	Age kyr	tot U ppm	cfb tot U ppm	Uauth ppm	cfb Uauth ppm	Th ppm	cfb Th ppm	Mo ppm	cfb Mo ppm	Cd ppm	cfb Cd ppm
8	7.30	2.03	7.88	0.96	3.72	2.24	8.70	0.19	0.74	0.48	1.86
22.5	9.95	2.50	7.20	1.49	4.29	2.81	8.09	0.22	0.63	0.56	1.61
35	12.30	2.38	5.77	1.42	3.44	3.38	8.20	0.25	0.61	0.60	1.46
55	16.00	4.77	11.29	3.96	9.37	3.82	9.04	0.29	0.69	0.72	1.70
65	17.85	3.43	7.93	2.69	6.21	3.50	8.09	0.29	0.67	0.73	1.69
74	19.51	2.73	6.09	1.90	4.25	3.90	8.71	0.29	0.65	0.36	0.80
82.5	21.07	2.83	6.38	2.09	4.71	3.49	7.86	0.22	0.50	0.56	1.26
95	23.43	3.39	7.98	2.66	6.26	3.43	8.07	0.29	0.68	0.70	1.65
105	25.28	2.82	6.84	2.05	4.97	3.63	8.80	0.31	0.75	0.44	1.07
115	27.15	2.11	5.18	1.46	3.58	3.06	7.51	0.29	0.71	0.47	1.15
125	29.00	2.52	6.38	1.87	4.73	3.06	7.75	0.25	0.63	0.97	2.46
135	30.83	3.30	8.80	2.64	7.04	3.10	8.27	0.29	0.77	0.84	2.24
145	32.69	2.96	8.22	2.20	6.12	3.31	9.19	0.29	0.81	0.41	1.14
162.5	35.96	3.17	8.71	2.56	7.04	2.86	7.86	0.34	0.93	1.04	2.86
171.5	37.67	3.56	9.79	2.94	8.09	2.92	8.03	0.39	1.07	0.63	1.73
181.5	39.57	3.48	9.90	2.90	8.25	2.74	7.80	0.37	1.05	0.52	1.48
191.5	41.47	3.47	8.98	2.72	7.03	3.55	9.18	0.38	0.98	0.62	1.60
201.5	43.36	3.14	7.31	2.40	5.59	3.49	8.13	0.36	0.84	0.76	1.77
211.5	45.26	3.51	9.07	2.86	7.39	3.07	7.93	0.34	0.88	1.55	4.01
221.5	47.16	3.59	9.73	2.98	8.07	2.88	7.80	0.76	2.06	0.63	1.71
231.5	49.06	3.92	10.20	3.32	8.64	2.83	7.37	1.11	2.89	1.12	2.92
241.5	50.96	3.22	8.05	2.50	6.26	3.38	8.45	0.30	0.75	0.68	1.70
253	53.15	2.52	5.93	1.80	4.23	3.41	8.03	0.30	0.71	0.51	1.20
263	55.05	2.58	5.62	1.88	4.09	3.32	7.24	0.29	0.63	1.08	2.35
271.5	56.66	2.22	4.59	1.26	2.61	4.29	8.86	0.28	0.58	0.40	0.83
281.5	58.56	2.16	4.02	1.11	2.06	4.61	8.58	0.32	0.60	0.29	0.54
291.5	60.48	2.38	4.17	1.41	2.48	4.55	7.97	0.35	0.61	0.61	1.07
313.5	64.73	4.01	8.38	2.80	5.84	5.72	11.96	0.60	1.25	0.64	1.34
322	66.35	4.20	8.69	3.04	6.30	5.45	11.28	0.57	1.18	0.61	1.26
332	68.30	4.45	8.79	3.10	6.12	6.37	12.58	0.78	1.54	0.80	1.58
342.5	69.96	4.04	7.39	2.51	4.59	7.22	13.21	0.84	1.54	0.67	1.23
352.5	71.30	3.98	6.05	1.81	2.76	10.20	15.51	1.16	1.76	0.48	0.73
362.5	72.67	3.90	7.48	2.69	5.17	4.91	9.42	0.75	1.44	0.69	1.32
371.5	73.85	4.02	10.72	2.76	7.37	4.70	12.53	0.73	1.95	0.78	2.08
382.5	75.26	3.96	10.65	1.91	5.14	8.38	22.54	1.05	2.82	0.59	1.59
392.5	76.58	3.77	9.78	2.81	7.30	3.05	7.91	0.56	1.45	0.97	2.52
402.5	77.95	3.33	10.25	2.44	7.52	2.44	7.51	0.56	1.72	0.54	1.66
412	79.22	2.63	9.65	1.74	6.37	2.18	8.00	0.50	1.83	0.87	3.19
422	80.52	2.13	7.91	1.18	4.39	2.20	8.17	0.52	1.93	0.40	1.49
432	81.85	1.77	5.57	0.82	2.60	2.42	7.62	0.37	1.17	0.38	1.20
443	83.33	1.48	4.39	0.43	1.26	3.72	11.05	0.35	1.04	0.29	0.86
451.5	84.47	1.44	4.55	0.49	1.55	3.67	11.60	0.37	1.17	0.42	1.33
460.5	85.67	2.63	8.93	1.70	5.79	3.44	11.68	0.33	1.12	0.61	2.07
470	86.92	3.19	11.53	2.45	8.86	2.44	8.82	0.33	1.19	0.46	1.66
480	88.27	4.31	15.96	3.54	13.10	2.54	9.41	1.10	4.07	0.64	2.37
490	89.62	3.58	12.62	2.87	10.13	2.15	7.58	0.38	1.34	0.99	3.49
500.5	90.98	3.36	11.87	2.64	9.33	2.22	7.84	0.46	1.63	0.52	1.84
510.5	92.34	3.45	13.58	2.67	10.52	2.26	8.90	0.46	1.81	0.83	3.27
520.5	93.68	2.92	11.45	2.30	9.03	1.57	6.16	0.54	2.12	0.52	2.04
530.5	95.04	2.85	10.75	2.13	8.03	2.13	8.04	0.47	1.77	0.53	2.00
540.5	96.38	2.99	11.68	2.23	8.70	2.24	8.75	0.42	1.64	0.69	2.70
550.5	97.68	2.94	11.76	2.18	8.70	2.15	8.60	0.44	1.76	0.86	3.44
560.5	99.04	3.03	10.17	2.29	7.68	2.22	7.45	0.45	1.51	0.59	1.98
570	100.32	2.31	7.71	1.53	5.11	2.32	7.74	0.62	2.07	0.65	2.17
580	101.62	2.47	7.48	1.57	4.74	2.86	8.67	0.48	1.45	0.38	1.15
590	102.97	2.36	6.32	1.50	4.03	2.52	6.75	0.40	1.07	0.53	1.42
600	104.30	2.52	6.81	1.63	4.39	2.58	6.97	0.43	1.16	0.43	1.16
611.5	105.83	3.56	9.71	2.68	7.30	3.18	8.67	0.55	1.50	0.51	1.39
621	107.12	3.58	10.50	2.82	8.27	2.71	7.95	0.60	1.76	0.68	1.99
631	108.45	4.79	15.81	3.97	13.10	2.47	8.15	0.67	2.21	1.19	3.93
641	109.79	4.32	15.08	3.51	12.27	2.38	8.31	0.74	2.58	0.78	2.72
653	111.35	3.76	13.29	2.87	10.16	2.57	9.08	0.70	2.47	0.74	2.61
660.5	112.36	3.50	11.67	2.66	8.87	2.33	7.77	0.74	2.47	0.77	2.57
670.5	113.72	3.12	10.80	2.31	7.98	2.11	7.30	0.70	2.42	0.80	2.77
680.5	115.02	3.09	11.70	2.31	8.75	1.99	7.54	0.61	2.31	0.68	2.58
690.5	116.32	2.71	10.07	1.90	7.06	2.11	7.84	0.66	2.45	0.67	2.49

Table 2. *(Continued)*

Depth cm	Age kyr	tot U ppm	cfb tot U ppm	Uauth ppm	cfb Uauth ppm	Th ppm	cfb Th ppm	Mo ppm	cfb Mo ppm	Cd ppm	cfb Cd ppm
700.5	117.66	2.82	10.56	2.01	7.53	2.01	7.53	0.49	1.84	0.69	2.58
710.5	119.01	2.59	8.95	1.76	6.08	2.22	7.67	0.58	2.00	0.52	1.80
723	120.61	2.82	10.00	1.87	6.64	2.19	7.77	0.53	1.88	0.65	2.30
730	121.55	2.67	8.78	1.63	5.38	2.32	7.63	0.41	1.35	0.62	2.04
740	122.89	2.83	8.46	1.71	5.10	2.50	7.47	0.30	0.90	1.04	3.11
750	124.19	2.58	7.38	1.42	4.07	2.77	7.93	0.51	1.46	0.68	1.95
760.5	125.57	2.54	6.84	1.36	3.65	3.26	8.77	0.26	0.70	0.88	2.37
769.5	126.77	2.69	7.29	1.66	4.51	3.08	8.35	0.23	0.62	0.43	1.17
779.5	128.26	2.66	7.58	1.76	5.01	2.94	8.38	0.26	0.74	0.54	1.54
787	129.49	2.66	7.28	1.89	5.17	2.82	7.72	0.31	0.85	0.56	1.53
797	131.17	4.64	12.04	4.04	10.48	2.84	7.37	0.40	1.04	1.02	2.65
805	132.50	6.13	16.51	5.51	14.83	2.94	7.92	0.38	1.02	1.77	4.77
815	134.10	5.31	13.53	4.73	12.06	2.72	6.93	0.54	1.38	1.11	2.83
825	135.74	4.41	11.17	3.78	9.59	2.95	7.47	0.49	1.24	0.72	1.82
835	137.40	4.17	11.01	3.57	9.42	2.84	7.50	0.61	1.61	0.94	2.48
845	139.03	4.38	11.27	3.74	9.62	3.02	7.77	0.68	1.75	0.94	2.42
855	140.70	4.00	9.97	3.35	8.36	3.04	7.58	0.55	1.37	0.91	2.27
865	142.33	3.04	6.83	2.35	5.29	3.23	7.26	0.52	1.17	0.59	1.33
880.5	144.88	2.22	5.75	1.38	3.57	2.92	7.56	0.37	0.96	0.40	1.04
889.5	146.33	2.35	7.09	1.35	4.06	2.74	8.26	0.35	1.06	0.38	1.15
899.5	147.95	2.08	5.97	1.18	3.40	3.06	8.78	0.39	1.12	0.25	0.72
911	149.83	1.93	4.64	1.03	2.48	3.97	9.53	0.33	0.79	0.32	0.77
921	151.46	2.42	5.54	1.59	3.63	3.74	8.56	0.36	0.82	0.46	1.05
931	153.12	2.77	6.60	2.15	5.11	2.94	7.00	0.42	1.00	0.53	1.26
941	154.76	3.89	9.15	3.12	7.35	3.17	7.46	0.46	1.08	0.87	2.05
951	156.36	3.79	9.15	3.09	7.46	3.02	7.29	0.42	1.01	0.67	1.62
961	157.98	3.68	9.08	2.96	7.29	3.41	8.41	0.37	0.91	0.59	1.46
971	159.63	4.09	9.91	3.33	8.06	3.59	8.70	0.43	1.04	0.96	2.33
981	161.50	3.94	10.00	3.31	8.40	2.96	7.51	0.29	0.74	1.01	2.56
991	163.50	2.62	7.42	2.00	5.67	2.91	8.24	0.32	0.91	0.58	1.64
1001	165.44	2.44	6.42	1.72	4.54	3.37	8.87	0.35	0.92	0.46	1.21
1008.5	166.90	2.08	5.07	1.27	3.09	3.53	8.61	0.42	1.02	0.45	1.10
1018.5	168.90	2.23	5.95	1.20	3.20	3.72	9.92	0.39	1.04	0.39	1.04
1024.5	170.10	3.00	9.52	2.26	7.16	1.86	5.90	0.25	0.79	0.56	1.78
1031	171.40	2.39	4.71	1.24	2.44	4.64	9.15	0.50	0.99	0.38	0.75
1038	172.76	2.74	4.70	1.68	2.87	5.01	8.59	0.64	1.10	0.81	1.39
1047.5	174.60	3.51	7.67	2.78	6.08	3.42	7.48	0.73	1.60	0.68	1.49
1058	176.70	3.42	7.99	2.73	6.38	3.25	7.59	0.84	1.96	0.89	2.08
1067	178.50	3.37	8.12	2.69	6.49	3.18	7.66	0.71	1.71	0.68	1.64
1077	180.50	3.88	10.93	3.11	8.76	3.07	8.65	0.95	2.68	0.77	2.17
1086.5	182.38	4.11	13.40	3.27	10.66	2.60	8.48	0.69	2.25	0.90	2.93
1096.5	184.33	3.62	11.57	2.75	8.79	2.51	8.03	0.70	2.24	0.69	2.21
1107	186.40	2.86	8.80	1.94	5.97	2.97	9.14	0.67	2.06	0.54	1.66
1117	188.65	2.95	9.37	2.08	6.61	2.71	8.60	0.53	1.68	0.66	2.10
1127	191.20	2.36	8.43	1.54	5.49	2.39	8.54	0.60	2.14	0.40	1.43
1137	193.75	1.89	6.94	1.15	4.21	2.10	7.71	0.29	1.06	0.37	1.36
1147.5	196.43	1.67	6.07	0.94	3.41	1.83	6.65	0.39	1.42	0.39	1.42
1158	199.12	3.09	11.93	2.18	8.40	2.44	9.42	0.40	1.54	1.47	5.68
1167.5	201.53	4.10	17.37	3.30	13.98	1.86	7.88	0.24	1.02	0.85	3.60
1178.5	204.35	2.99	11.49	2.22	8.54	1.65	6.34	0.30	1.15	0.72	2.77
1188.5	206.92	3.07	12.66	2.26	9.33	1.44	5.94	0.26	1.07	0.88	3.63
1198.5	209.48	2.58	11.56	1.68	7.53	1.50	6.72	0.24	1.08	0.67	3.00
1208.5	212.03	2.38	8.72	1.50	5.48	1.64	6.01	0.28	1.03	0.57	2.09
1217.5	214.33	2.05	6.10	1.21	3.60	2.21	6.58	0.24	0.71	0.70	2.08
1228	217.00	1.68	4.02	0.89	2.14	3.22	7.71	0.29	0.69	0.48	1.15
1237.5	219.47	1.88	4.59	1.13	2.76	3.52	8.59	0.34	0.83	0.40	0.98
1247.5	222.03	2.86	8.32	2.08	6.05	3.68	10.71	0.27	0.79	1.07	3.11
1257.5	224.57	4.14	13.56	3.47	11.36	2.54	8.32	0.49	1.61	0.70	2.29
1267.5	227.13	3.56	14.35	2.68	10.79	2.27	9.15	0.36	1.45	0.63	2.54
1277.5	229.67	3.12	14.67	2.19	10.28	1.77	8.32	0.49	2.30	0.61	2.87
1287.5	232.27	2.78	12.19	1.86	8.16	1.74	7.63	0.43	1.89	0.66	2.89
1297.5	234.83	2.47	10.65	1.55	6.68	1.91	8.23	0.38	1.64	0.55	2.37
1307.5	237.37	2.28	9.27	1.40	5.69	1.91	7.76	0.57	2.32	0.63	2.56
1317.5	239.99	1.97	6.47	1.08	3.57	3.00	9.86	0.29	0.95	0.40	1.31
1329	243.01	2.67	7.84	2.08	6.09	2.80	8.22	0.31	0.91	0.76	2.23

Table 2. *(Continued)*

Depth cm	Age kyr	tot U ppm	cfb tot U ppm	Uauth ppm	cfb Uauth ppm	Th ppm	cfb Th ppm	Mo ppm	cfb Mo ppm	Cd ppm	cfb Cd ppm
1338	245.55	3.76	10.73	3.15	8.98	2.88	8.22	0.41	1.17	0.99	2.82
1348.5	248.85	4.40	13.44	3.77	11.51	2.97	9.07	0.40	1.22	0.98	2.99
1358	251.94	3.47	10.80	2.90	9.02	2.69	8.37	0.37	1.15	0.61	1.90
1368	255.14	3.60	10.89	3.10	9.38	2.36	7.14	0.52	1.57	0.67	2.03
1379	258.66	2.47	7.23	1.84	5.39	2.97	8.70	0.30	0.88	0.65	1.90
1388	261.54	2.15	5.66	1.50	3.95	3.07	8.08	0.34	0.90	0.54	1.42
1398	264.79	2.12	4.68	1.24	2.74	4.15	9.17	0.36	0.80	0.53	1.17
1409	268.35	1.86	3.85	0.93	1.94	4.36	9.04	0.35	0.73	0.31	0.64
1419	271.55	2.38	5.01	1.47	3.09	4.30	9.05	0.33	0.69	0.35	0.74
1428	274.44	3.68	8.03	2.83	6.18	3.98	8.68	0.55	1.20	0.61	1.33
1438	277.64	3.94	9.91	3.15	7.92	3.12	7.85	0.53	1.33	0.86	2.16
1448	280.85	3.60	11.25	2.81	8.79	2.61	8.16	0.50	1.56	0.75	2.34
1458	283.35	2.93	11.68	2.25	8.96	2.21	8.81	0.59	2.35	0.59	2.35
1467	285.04	2.85	11.72	2.16	8.88	2.01	8.27	0.44	1.81	0.75	3.08
1479	287.28	2.29	8.64	1.42	5.36	2.59	9.77	0.32	1.21	0.64	2.42
1490	289.35	2.17	7.24	1.32	4.40	2.44	8.14	0.39	1.30	0.46	1.53
1499	291.06	2.29	6.91	1.58	4.76	2.53	7.64	0.33	1.00	0.38	1.15
1509.5	293.04	2.39	7.60	1.84	5.84	2.61	8.30	0.35	1.11	0.39	1.24
1519	294.85	3.17	12.60	2.76	10.98	1.93	7.67	0.38	1.51	0.94	3.74
1528.5	296.65	2.68	12.79	2.17	10.35	1.78	8.50	0.38	1.81	0.64	3.06
1538	298.45	3.28	16.40	2.72	13.62	1.38	6.90	0.46	2.30	0.69	3.45
1548.5	300.40	2.56	13.89	1.98	10.75	1.41	7.65	0.43	2.33	0.51	2.77
1559	302.35	2.80	13.43	2.19	10.52	1.72	8.25	0.81	3.88	0.68	3.26
1569	304.25	2.88	12.06	2.11	8.85	2.52	10.55	0.55	2.30	0.57	2.39
1581	306.54	2.45	10.38	1.76	7.45	1.89	8.01	0.88	3.73	0.61	2.58
1591	308.45	2.62	11.55	1.90	8.36	2.15	9.48	0.51	2.25	0.43	1.90
1601	310.35	2.46	10.17	1.91	7.89	2.10	8.68	0.49	2.02	0.77	3.18
1611	312.25	2.18	8.13	1.59	5.91	2.22	8.28	0.54	2.01	0.44	1.64
1621	314.09	2.96	11.33	2.21	8.47	2.53	9.68	0.52	1.99	0.66	2.53
1631	315.95	3.68	16.34	3.00	13.32	1.74	7.72	0.52	2.31	0.66	2.93
1641	317.85	3.28	17.40	2.56	13.59	1.61	8.54	0.54	2.86	0.87	4.62
1651	319.75	3.07	19.04	2.44	15.13	1.24	7.69	0.52	3.22	0.79	4.90
1661	321.65	3.06	20.78	2.46	16.69	1.12	7.61	0.56	3.80	0.86	5.84
1671	323.55	2.84	16.73	2.27	13.38	1.21	7.13	0.63	3.71	0.68	4.01
1681	325.45	2.74	12.92	2.18	10.26	1.56	7.36	0.38	1.79	0.85	4.01
1691	327.35	1.94	7.87	1.38	5.60	1.81	7.34	0.45	1.83	0.49	1.99
1701	329.25	1.58	6.64	0.89	3.74	2.23	9.37	0.49	2.06	0.49	2.06
1711	331.15	1.86	7.42	1.11	4.43	2.56	10.21	0.40	1.60	0.48	1.91
1720	332.86	2.08	6.91	1.29	4.30	3.19	10.60	0.38	1.26	0.54	1.79

ate-free basis to account for the effect of dilution by carbonate (also available in Table 2).

Authigenic U (U_{auth}) concentrations were calculated by subtracting a crustal component determined from the measured Th concentration and a detrital Th/U weight ratio of 4.71 (Taylor and McLennan, 1985). Aragonite contributed by the nearby Maldives platform is an additional source of detrital U. Sediments from core MD900963 contain up to 20% of bank-derived aragonite on a total sediment basis, with the most-elevated intervals corresponding to high sea level stands that flooded the platform (Haddad, 1994). Platform-derived detrital U was estimated by assuming a U content of 3 ppm in coral aragonite. The total detrital U correction averages 2.5 ppm, compared to an average U concentration of ~9.4 ppm (carbonate-free basis). Figure 3c clearly shows that U and U_{auth} profiles are roughly parallel and that the two records exhibit the same variability. Therefore, using the U or U_{auth} profile would not change the discussion below.

U_{auth} concentrations range between 1 and 17 ppm in the core (Fig. 3c). Particularly striking is a series of well-defined cycles from 340 to 80 ka with an average separation between peaks of 23 kyr. This cycle closely follows variations in the precessional

index, with maxima in U_{auth} (Fig. 3c) corresponding to minima in summer insolation as indicated by high values of precession index (Fig. 3a) in the Northern Hemisphere (June insolation at 30°N and 0°) (Berger and Loutre, 1991). The U_{auth} cycles are not as well defined in the upper 5 m of the core, which include the Toba ash layer.

Cd concentrations on a carbonate-free basis range from 0.5 to 6 ppm (Fig. 3d) and are significantly above the mean crustal level of 0.1 ppm (Taylor and McLennan, 1985). Four elevated values (> 4 ppm) correspond to sediment deposition dates of 322, 199, 132, and 45 ka. Many of the variations in Cd concentrations parallel the U_{auth} cycles, although the cyclicity is less well defined for Cd.

Mo concentrations on a carbonate-free basis vary between 0.5 and 4 ppm in the core, with several broad maxima at 330, 310, 280, 235, 180, 130, 88, 75 to 70, and 49 ka (Fig. 3e). Mo concentrations are usually within the 1 to 2.6 ppm range reported for the continental crust (Taylor and McLennan, 1985). The Mo peak at 75 to 70 ka coincides with the Th-enriched layer of Toba ash. It is worth noting that several of the prominent U_{auth} and Cd cycles, particularly those at 210 and 160 ka, are not mirrored in the Mo data.
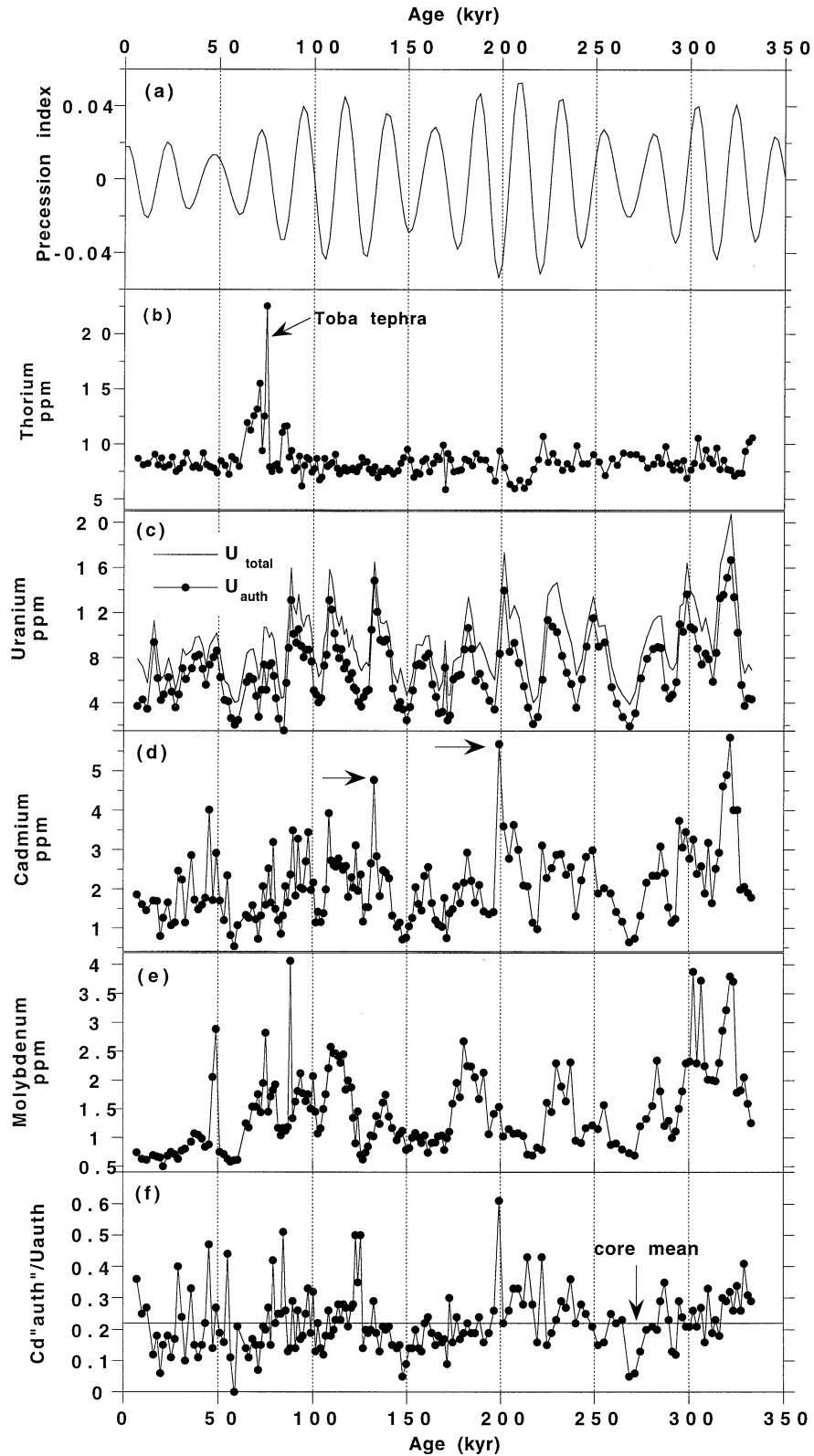
Fig. 3. Trace elements on a carbonate-free basis for the last 350 kyr in core MD900963: (a) precession index (Berger and Loutre, 1991); (b) Th concentration; (c) U (solid line without dots) and U_{auth} (solid line with dots), see text for details on the calculations; (d) Cd; (e) Mo; (f) $(Cd/U)_{auth}$ ratio. Data for U, Th, U_{auth}, Mo, and Cd are given in Table 2 (total concentrations and concentrations on a carbonate-free basis). Arrows in (d) highlight examples of maxima of Cd probably due to postdepositional remobilization.

Table 3. Concentrations of total C37 alkenones (tot C37) and organic carbon (OC).

Depth cm	Total C37 μg/g	OC %	Depth cm	Total C37 μg/g	OC %	Depth cm	Total C37 μg/g	OC %	Depth cm	Total C37 μg/g	OC %
1		0.62	475	1.83	0.50	945	2.14	0.50	1379	1.13	0.56
11		0.46	485	2.79	0.55	955	3.08	0.58	1388	0.99	0.55
21		0.50	495	2.08	0.43	965	2.21	0.51	1398	0.52	0.47
31		0.54	505	3.36	0.52	975	2.17	0.51	1409	0.32	0.36
41	0.81	0.79	515	1.62	0.39	985	1.51	0.45	1419	1.28	0.54
51	1.08	0.87	525	1.84	0.44	995	0.90	0.43	1428	1.55	0.51
61	1.06	0.79	535	1.74	0.49	1000	1.22	0.35	1438	3.45	0.63
71	0.71	0.67	545	1.53	0.44	1005	0.66		1448	0.46	0.59
81	0.72	0.73	555		0.49	1010	0.46	0.44	1458	0.79	0.61
91	0.85	0.74	565	1.13	0.43	1015	0.94		1467	1.02	0.49
101	0.58	0.62	575	1.08	0.43	1024	2.25	0.62	1479	3.76	0.73
111		0.77	585	0.63	0.34	1029	1.76	0.63	1490	3.01	0.67
121	0.71	0.64	595	0.85	0.40	1037	3.42	0.91	1499	1.36	0.50
131	0.60	0.63	609	0.92	0.39	1047	1.98	0.53	1509.5	1.56	0.43
141		0.63	625	2.41	0.56	1057.5	3.86	0.63	1519	1.80	0.50
150	0.47	0.57	635	2.24	0.54	1066.5	5.14	0.63	1528.5	1.55	0.52
161	0.97	0.62	645	1.67	0.52	1076.5	6.44	0.72	1538.5	2.12	0.54
171	0.97	0.64	655	2.99	0.53	1086	5.08	0.79	1549	1.52	0.58
181	0.84	0.59	665	2.53	0.53	1096	6.70	0.77	1559	1.89	0.76
191	0.83	0.60	675	1.75	0.40	1106.5	2.05	0.60	1569	1.74	0.55
201	0.86	0.56	685		0.37	1116.5	2.88	0.60	1581	1.74	0.57
211	1.05	0.61	695	1.00	0.38	1126.5	1.87	0.57	1591	1.89	0.57
221	0.88	0.57	705	0.77	0.37	1136.5	0.46	0.45	1601	0.75	0.49
231	0.93	0.58	715		0.41	1147	0.81	0.58	1611	0.52	0.51
241	0.78	0.57	725	0.48	0.44	1157.5	1.93	0.53	1621	1.08	0.44
245	0.84		735	0.32	0.32	1167	2.40	0.67	1631	2.69	0.62
251		0.61	745		0.32	1178.5	2.27	0.47	1641	1.83	0.56
261	0.67	0.53	757.5		0.35	1188.5	1.90	0.39	1651	2.40	0.65
271	0.33	0.40	765	0.50	0.31	1198.5	1.46	0.72	1661	1.72	0.62
281	0.41	0.48	775		0.26	1208.5	1.01	0.71	1671	1.75	0.61
291	0.56	0.63	785	0.74	0.39	1217.5	0.75	0.70	1681	0.96	0.54
300	0.83	0.73	795		0.50	1228	0.50	0.46	1691	0.47	0.61
327	1.84	0.63	805	3.12	0.69	1237.5	0.64	0.37	1701	0.28	0.32
337	1.57	0.56	815	3.85	0.68	1247.5	1.48	0.40	1711	0.29	0.37
347		0.46	825	3.46	0.69	1257.5	2.94	0.62	1720	0.67	0.57
359	1.46	0.53	835	3.59	0.81	1267.5	2.54	0.67	1728	0.27	0.18
367	1.50	0.55	845	4.24	0.77	1277.5	3.50	0.69	1735.5	1.35	0.38
377	1.32	0.50	855	2.90	0.66	1287.5	2.12	0.53	1744	3.49	0.54
387	1.85	0.55	865	0.94	0.56	1297.5	1.93	0.48	1756.5	6.06	0.59
397	1.49	0.54	875	0.98	0.49	1307.5	1.69	0.48	1766.5	2.94	0.54
407	1.19	0.49	885	0.63	0.38	1317.5	0.24	0.38	1770.5	4.76	0.54
417	1.01	0.47	895		0.28	1329	0.68	0.53	1785.5	1.63	0.42
427	0.58		906	0.59	0.32	1338	2.01	0.58	1796	1.46	0.38
447		0.38	915	1.04	0.39	1348.5	3.69	0.77	1806	1.73	0.40
457		0.34	925	1.54	0.47	1358	2.19	0.67	1810.5	1.69	0.40
465	1.36	0.48	935	1.83	0.50	1368	2.44	0.77			

3.2. Organic Constituents

The extended OC data vary between 0.3 and 0.8%, a range comparable to that obtained by Rostek et al. (1997) for the upper of 10 m of the core (Fig. 2b; Table 3). These concentrations are significantly lower than in sediment records from the oxygen minimum zone (OMZ) of the northern Arabian Sea (Schulz et al., 1998). The OC profile is well correlated with the $\delta^{18}O$ record, with the highest OC levels associated with glacial $\delta^{18}O$ maxima. The extension of the $totC_{37}$ record is also within the 0.2 to 7 μg/g range of the previously published data (Fig. 2c; Table 3). The OC record contains a 23-kyr cycle, although the pattern is better defined by the $totC_{37}$ data. The correlation between the OC and $totC_{37}$ records suggests that both reflect changes in marine productivity rather than changes in the input of terrestrial carbon. As in the case of authigenic metal con-

centrations, maxima in OC and $totC_{37}$ correspond to minima in summer insolation for the Northern Hemisphere (Fig. 3a).

4. DISCUSSION

4.1. Changes in the Sedimentary Environment and the Deposition Processes

4.1.1. The redox state of the sediment indicated by U and Mo

At least a significant fraction of authigenic U in core MD900963 is likely to be derived from reductive precipitation driven by organic carbon flux to the sediment, because the contribution from surface-derived particulate nonlithogenic U is likely to be small at the present bottom water dissolved oxygen level (Zheng et al., 2001b). The low end of total U

concentrations measured in core MD900963 is equivalent to total U concentrations of ~2 ppm in the upper 15 cm of the sediment at a number of oxic sites, including the MANOP S site (Klinkhammer and Palmer, 1991; sedimentation rate = 0.3 cm/kyr) and the mesotrophic EUMELI (sedimentation rate = 1.5 cm/kyr) sites of the northeast tropical Atlantic (Legeleux et al., 1994). Concentrations of 2 to 5 ppm of total U measured in suboxic areas of the NE African margin (sedimentation rate = 4.4 cm/kyr; Legeleux et al., 1994) are similar to the high end of the range of U concentrations in core MD900963. Both the mesotrophic and suboxic NE African sites are overlaid by well-oxygenated waters (140–150 μmol/L; Levitus and Boyer, 1994a) with PP in the region ranging between 125 and 180 gC/m^2/yr (Legeleux et al., 1994). Such conditions appear to span the full amplitude of redox conditions recorded in core MD900963 during the past 330 kyr. Evidently conditions in the sediments of the eastern Arabian Sea at the depth of MD900963 never became as reducing as the OMZ on the western slope of India (3–7.5 ppm of raw U; Nagender et al., 1997). Such comparisons are justified, since the sedimentation rates in core MD900963 are comparable to that of the other sites. However, a more precise assessment would require a comparison of U_{auth} mass accumulation rates on a carbonate-free basis (Anderson, 1987; Barnes and Cochran, 1990; Klinkhammer and Palmer, 1991).

Total Mo concentrations below 0.6 ppm in MD900963 (i.e., below 4 ppm on a carbonate-free basis) rule out strongly reducing conditions in the eastern Arabian Sea. Conditions similar to the Black Sea or the Cariaco Trench, where sediments contain 20 to 60 ppm Mo (Emerson and Huested, 1991; Crusius et al., 1996) were clearly never reached at the core site (Zheng et al., 2000). Considerable Mo enrichments have been observed in other regions within the Arabian Sea that are more reducing. Sediment deposited over the past 300 kyr within the OMZ of the Oman margin contain between 2 and 23 ppm of total Mo (ODP 724C; Shimmield, 1992), for instance, whereas sediment in the OMZ ($O_2 < 5$ μmol/L) of the Indian Margin contain up to 30 ppm of total Mo (Sirocko, 1995). Instead, the Mo record for MD900963 suggests conditions similar to the suboxic eutrophic and mesotrophic sites of the NE African margin (0.4–2 ppm of total Mo; Legeleux et al., 1994), the well-oxygenated Japan Sea, and the ventilated region of Saanich Inlet (1–2 ppm of total Mo; Crusius et al., 1996). Unlike Sarkar et al. (1993), we see no evidence that water below 2000 m off the west coast of India became anoxic during the Last Glacial Maximum (LGM).

Cyclic variations in Mo concentrations in MD900963 could also be linked to Mn cycling since coprecipitation with Mn oxides can lead to elevated concentrations (up to 21 ppm of raw Mo) under fairly oxic conditions (Shimmield and Price, 1986). However, this mechanism would not explain Mo peaks that correlate with Cd and U peaks, since the Mn oxides should have been reduced before Cd and U could accumulate.

4.1.2. OC, totC$_{37}$, and authigenic metals accumulation driven by organic matter accumulation and remineralization

Variations in U_{auth}, Cd, and to some extent, Mo concentrations are positively correlated with the organic constituents OC

Table 4. Correlation coefficients matrix between organic constituents and metals for the 330-0 ka period ($n = 170$). Metal concentrations are expressed on a carbonate-free basis. All correlations with coefficients > 0.3 are statistically significant with p < .0001.

	totC37	Corg	Uauth	Mo
Cd	0.30	0.18	0.79	0.50
Mo	0.33	0.09	0.59	
Uauth	0.50	0.35		
Corg	0.52			

and totC$_{37}$ (Figs. 2 and 3). The sedimentary environment at site MD900963 alternated in a 23-kyr cycle between an oxic state, when accumulation of authigenic metals, OC, and totC$_{37}$ was low, and a suboxic state, when accumulation of the same constituents was high. Relationships between the different pairs of proxies were determined by linear regression for the 330- to 0-kyr period for confirmation (Table 4). For these regressions ($n = 170$), all correlation coefficients >0.3 are highly significant (p < 0.0001). Variations in OC and totC$_{37}$ concentrations are well correlated (r = 0.52). Variations in authigenic metal concentrations are significantly correlated with totC$_{37}$ (Table 4). The best of these correlations is between U_{auth} and totC$_{37}$ (r = 0.50). The best correlation between two metals is for U_{auth} and Cd (r = 0.79), confirming the similarity of the environmental conditions required to drive sedimentary enrichment for U and Cd (Rosenthal et al., 1995a,b).

The organic and metal records closely track two independent paleoproductivity proxies measured in the same core (Fig. 2d), the first based on coccolith assemblages (Beaufort et al., 1997) and the other on planktonic foraminifera (Cayre et al., 1999). The correspondence strongly suggests that a 23-kyr cycle in PP above site MD900963 primarily drove the recorded proxy variations. An increased flux of organic matter would indeed increase the oxidant demand at the water/sediment interface, thereby steepening the redox gradient in the sediment and increasing the accumulation of authigenic metals (Anderson, 1987; Barnes and Cochran, 1990; Klinkhammer and Palmer, 1991; Rosenthal et al., 1995a). Increased oxidation of organic matter to carbon dioxide should also have increased the generation of metabolic acids in the sediment and, therefore, carbonate dissolution (Emerson and Bender, 1980). Indeed, the index of foraminifera shell fragmentation shows higher shell dissolution during periods of high organic matter and metal accumulation (Fig. 2e). Our data cannot rule out, however, the potential amplification of the effect of enhanced productivity on authigenic metal accumulation due to a resulting decrease in bottom water oxygen. In addition, the interpretation of the U_{auth} record as solely driven by benthic processes may be an oversimplification. The contribution of particulate nonlithogenic U (PNU) should be on the order of 10% of the authigenic uranium if the bottom water dissolved oxygen concentration is ~140 μmol/L (Zheng et al., 2001a). However, paleoproductivity changes could have enhanced this contribution both by leading to higher PNU influx and to better PNU preservation linked to more reducing conditions. In any case, both types of U_{auth} should be positively correlated with the productivity. It remains difficult to separate the past fluctuations of both contributions, which probably exhibited the same cyclicity as primary productivity changes.

4.1.3. Mobility of authigenic metals

Although the metal and organic records are in phase and dominated by 23-kyr cycles, there are some systematic discrepancies. Particularly during isotopic stage 6.2, 132 kyr ago, maximum Cd concentrations are a few samples (i.e., a few tens of cm) above OC, totC$_{37}$, and U$_{auth}$ maxima, which do match each other. Similar offsets have been attributed to the migration of redox fronts (Wilson et al., 1985; Wallace et al., 1988; Rosenthal et al., 1995a; Thomson et al., 1998). The shape of the Cd and U$_{auth}$ peaks is also distinctly asymmetric, whereas peaks in organic proxies and the insolation curve are not. Rosenthal et al. (1995a) attributed the asymmetric shape of Cd and U peaks to remobilization and showed that Cd was more sensitive to this process than U. The explanation proposed by Rosenthal et al. (1995a) is that when the flux of OC diminishes, oxygen penetrates deeper into the sediment, thereby causing redissolution and diffusion of authigenic metals. Since Cd appears to be more sensitive to such mobilization by "burn-down" than U, Rosenthal et al. (1995a) also suggested that (Cd/U)$_{auth}$ ratios can provide a qualitative indication of post-depositional redistribution. By considering porewater data from different environments, Rosenthal et al. (1995b) calculated that the flux ratio of Cd to U removal averages 0.2 under steady state and, therefore, that Cd to U flux ratios >0.2 to 0.3 indicate remobilization. Cd data measured on MD900963 do not allow an explicit separation of detrital vs. authigenic Cd used to calculate accurate (Cd/U)$_{auth}$ ratios. However, to mimic this useful approach, a constant detrital background was subtracted from bulk Cd values to calculate (Cd/U)$_{"auth"}$ values (the lowest Cd content in Table 2 was used). Keeping this caveat in mind, it is worth noting that (Cd/U)$_{"auth"}$ ratios in MD900963 average 0.2, with higher values corresponding to Cd maxima deposited at 222, 199, 122, 85, and 80 ka and during the past 55 kyr (Fig. 3c). Within these intervals, Cd concentrations above 3 ppm could, therefore, reflect postdepositional redistribution rather than enhanced accumulation.

4.2. Paleoceanographic Implications

4.2.1. Could the observations be explained by changes in ventilation?

Substantial changes in the chemistry and circulation of the Indian Ocean since the LGM have been reported, and some of these changes could be relevant to earlier periods covered by core MD900963. Although the definition of the most recent 23-kyr cycles is not as good as further downcore, the LGM clearly corresponds to a period of higher accumulation of organic and metal indicators compared to the late Holocene. Interestingly, higher concentrations of U$_{auth}$ during the LGM compared to the Holocene have been reported for the Indian Ocean sector of the Southern Ocean (Rosenthal et al., 1995b; François et al., 1997) and a region north of the polar front in the South Atlantic (Kumar et al., 1995). The increase in U$_{auth}$ observed in glacial Subantarctic sediments, particularly in areas where productivity proxies do not suggest export flux of OC during the LGM, has been attributed to reduced ventilation of glacial Antarctic bottom water (Rosenthal et al., 1995b; François et al., 1997).

Because the site of core MD900963 is influenced today by ventilation in the Southern Ocean, the possibility that variations in U$_{auth}$ and Cd in the eastern Arabian Sea are linked through this process must be evaluated. There is conflicting evidence regarding changes in ventilation of the deep Indian Ocean below 2500 m (Boyle, 1992; Rosenthal et al., 1997; McCorkle et al., 1998). There is evidence of increased ventilation during the LGM of intermediate water masses (above 2000 m) of the northern Indian Ocean, however, which could have affected the site of core MD900963. Glacial benthic foraminiferal δ^{13}C and Cd/Ca ratios both suggest a reduction in the nutrient content of intermediate water in the northern Indian Ocean (Boyle, 1992), which is attributed to higher ventilation (Kallel et al., 1988) or a greater contribution of Atlantic origin water (Boyle et al., 1995). Such variations would have led to reduced preservation of organic constituents and authigenic metals during the LGM, which is the opposite of what is observed in core MD900963.

Further evidence against a dominant role of deep-water chemistry for the MD900963 records is that complete control by changes in ventilation should have resulted in decreased degradation of organic matter, hence, decreased dissolution of foraminifera, during periods of high OC, or vice versa. (Note that the core, being about 1 km above the lysocline, carbonate dissolution is probably related to respiration within the sediments.) Instead, the records clearly show enhanced dissolution of foraminifera during periods of high OC and authigenic metal accumulation.

An alternative way to constrain past changes of the ventilation would be to measure δ^{13}C or Cd/Ca in the benthic foraminifera from core MD900963. Willamowski et al. (2001) recently measured Cd/Ca in shells of *Uvigerina spp.* and *Cibicidoides wuellerstorfi* picked in core MD900963 within and outside several PP maxima as reconstructed with coccoliths. The main outcome is that the Cd/Ca values are relatively stable with no obvious relationship with the productivity proxies, which confirms that bottom water conditions did not drive the 23-kyr cyclicity observed in the organic and trace-element records.

4.2.2. How representative are productivity changes recorded at MD900963?

Today, the elevated productivity of various regions of the Arabian Sea is attributed to a series of mechanisms, all driven by wind patterns. Coastal upwelling driven by the summer monsoon, as well as Ekman pumping associated with the Find-later jet, have been invoked to explain increased productivity in the western Arabian Sea during summer (Nair et al., 1989; Ittekot et al., 1992; Haake et al., 1996). The summer monsoon also increases productivity along the west coast of India in response to wind- or current-induced upwelling (Sastry and D'Souza, 1972; Sharma, 1978; Naidu et al., 1992, 1999). In contrast, enhanced biologic productivity in the northwestern Arabian Sea appears to be driven by surface mixing during the winter monsoon (Banse and McClain, 1986; Nair et al., 1989; Madhupratap et al., 1996). Finally, late summer surface mixing and productivity maxima in the eastern equatorial Arabian Sea have been attributed to inter-monsoon westerlies (Beaufort et al., 1997, 1999).

Several authors have studied deep-sea sediment cores to document past conditions in these areas (Prell 1984; Fontugne and Duplessy 1986; Murray and Prell, 1992; Reichart et al., 1997, 1998; Rostek et al., 1997; Beaufort et al., 1997; Schubert et al., 1998). For the western part of the Arabian Sea, the
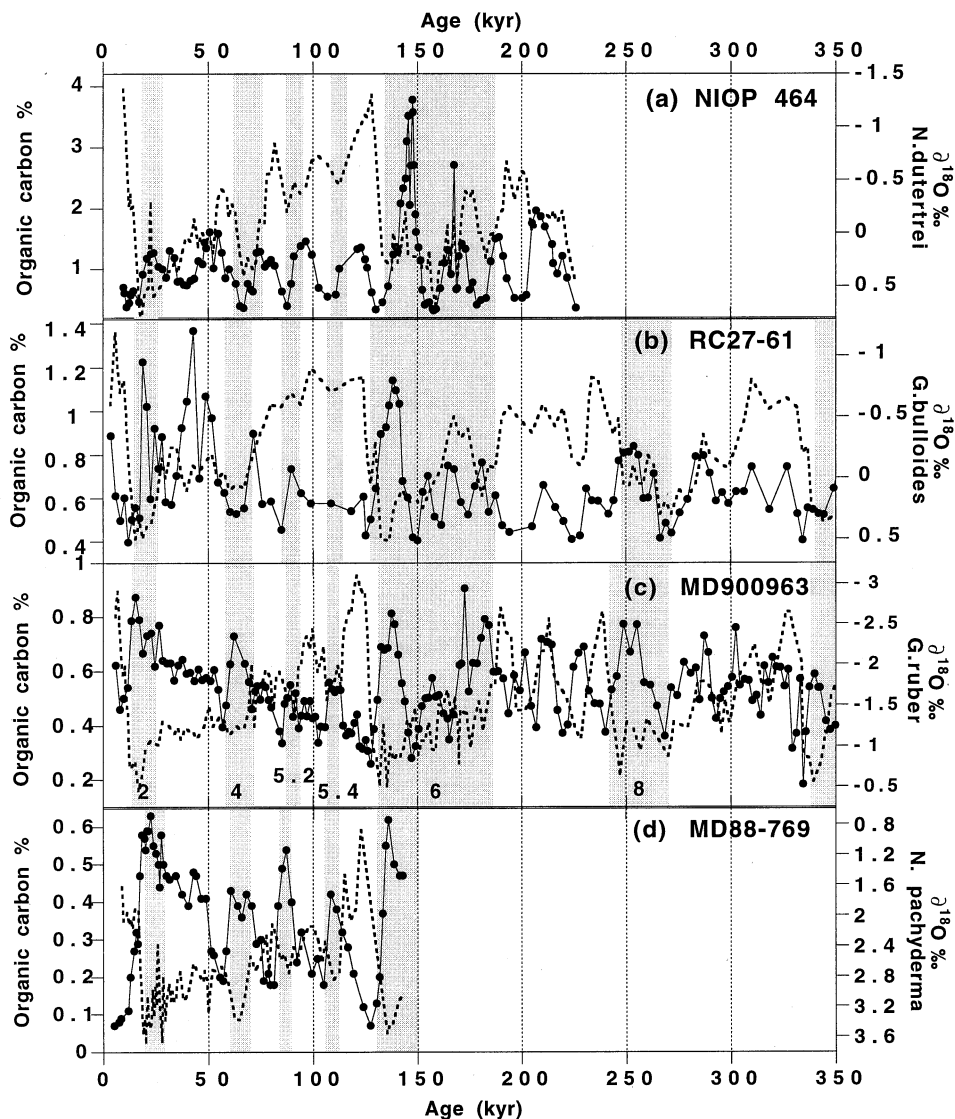
Fig. 4. Comparison between the variations of the sedimentary OC content (plain line with dots) in the equatorial Arabian Sea and other locations in the Indian Ocean. $\delta^{18}O$ stratigraphy (dashed line) is also reported for each core to enable comparisons independently of the age model: (a) Northern Arabian Sea, core NIOP 464 (22°15′N; 63°35′E; 1470 m water depth). The $\delta^{18}O$ record is obtained from the planktonic foraminifera *Neogloboquadrina dutertrei* (Reichart et al., 1998); (b) Oman Margin, RC27-61 (16°37′N; 59°51′E; 1893 m water depth) (Murray and Prell, 1992) and $\delta^{18}O$ record of *Globigerinoides sacculifer* (Clemens and Prell, 1990); (c) equatorial Arabian Sea, core MD900963, this study; and (d) sub-Antarctic Indian Ocean, core MD88-769 (46°04′S; 90°07′E; 3420 m water depth) and oxygen isotope record of *Neogloboquadrina pachyderma s.* (Rosenthal et al., 1995a). The shaded areas indicate the isotope glacial stages. They are labeled from core MD900963 $\delta^{18}O$ record. The time scale used for the core NIOP464 is that of Reichart et al. (1998). Glacial isotopic stages are shaded for each core to facilitate comparison of the profiles, despite some second-order discrepancies in the chronologies published in the original papers.

common wisdom is that geochemical records are controlled by a summer monsoon-productivity connection (e.g., Fontugne and Duplessy, 1986). However, other zones of the Arabian Sea may not behave in a similar fashion. In addition, shallow and deeper records are clearly different in some cases. For example, Schulte et al. (1999) have shown that organic compound records from the center of the OMZ in the Arabian Sea, unlike the deeper records from various locations of the Indian Ocean compared in the present paper,

predominantly reflect preservation (i.e., OMZ intensity) rather than productivity.

To determine the relative importance of these mechanisms in the past, we compared the productivity record of core MD900963 to three other well-documented cores located well below today's OMZ in different areas of the Indian Ocean (Figs. 1 and 4): core NIOP464 in the northern Arabian Sea (Reichart et al., 1997, 1998), core RC27-61 in the western Arabian Sea (Murray and Prell, 1992), and core
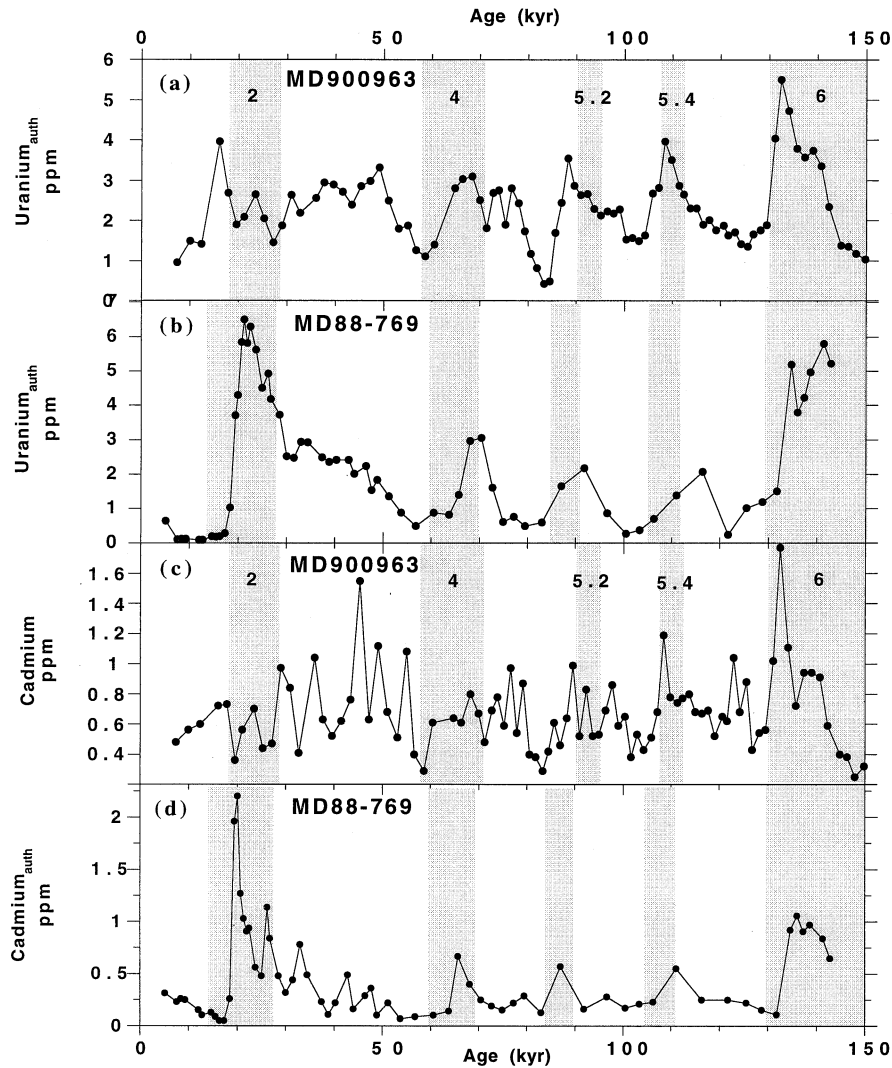
Fig. 5. Comparison between the variations of concentrations in U (a,b) and Cd (c,d) measured in cores MD900963 (this work) and MD88-769 (Rosenthal et al., 1995a). The shaded areas indicate isotope stages in both core chronologies (no adjustment was made to cancel second-order chronological differences). Note that concentrations are expressed vs. the total sediment as provided in tables from Rosenthal et al. (1995a). This comparison suggests correlated U and Cd peaks during isotope stages 6, 5.4, 5.2, and 4. This exercise is a first-order approximation only, since U_{auth} and Cd_{auth} from Rosenthal et al. (1995a) are truly extracted from the authigenic fraction, whereas data for MD900963 are based on assumed corrections for U_{auth} and total Cd values.

MD88-769 in the Subantarctic Indian Ocean (Rosenthal et al., 1995b). We use OC profiles for this comparison because this proxy is available at all sites. Independent measures of productivity are available for each of these cores and suggest that OC is a reasonable proxy for surface productivity.

Visual comparison shows striking similarities among certain sections of the four OC records. The OC records of the northern and eastern equatorial Arabian Sea are dominated by a 23-kyr cycle and although the NIOP464 record seems to slightly lead MD900963, both profiles show high productivity during high $\delta^{18}O$ intervals. In addition, maxima in OC concentrations in all three cores appear to correspond during stages 6, 5.2, and the end of 5.1, the middle of stage 3, and the last glacial stage 2. These correspondences suggest that changes in productivity, which were particularly well re-

corded in core MD900963, may be representative of much of the Indian Ocean.

4.2.3. Were 23-kyr productivity cycles driven by the monsoon?

Geologic records of productivity in the western and northern Arabian Sea are usually interpreted in terms of summer monsoon forcing (Prell, 1984; Fontugne and Duplessy, 1986; Sirocko et al., 1993). In agreement with climate models (Kutzbach and Guetter, 1986; Luther et al., 1990; Prell and Kutzbach, 1992), these records show a strengthened summer monsoon in phase with high boreal summer insolation (low precession index), due to the associated increase in land-sea temperature contrast.

Assuming that the summer monsoon did indeed respond as predicted by the models, our study suggests an opposite relation between OC accumulation in most of the Indian Ocean and the strength of the summer monsoon. In other words, our records suggest that the summer monsoon did not control PP over this entire region. This is not unexpected since productivity outside of the immediate area of coastal upwelling is inhibited during strong summer monsoons by a negative wind-stress curl (Luther et al., 1990).

There are other plausible wind-driven mechanisms that could explain changes in productivity over much of the Indian Ocean, such as changes in the seasonality of maximum productivity due to intermonsoon equatorial westerlies (Beaufort et al., 1997, 1999) or changes in mixing driven by the winter monsoon (Madhupratap et al., 1996; Rostek et al., 1997; Schubert et al., 1998), which may play a role in certain regions of the Indian Ocean. Similarities today between the seasonal cycle of changes in mixed-layer depth in the eastern Maldives and in the northern Arabian Sea (Rao et al., 1989), combined with the similar downcore OC profiles from these areas (Fig. 4) seem to support a winter monsoon linkage in this area. It is worth noting, however, that sediment traps moored in the eastern Arabian Sea and satellite-based pigment distributions indicate that, at least today, PP in the eastern part of the Arabian Sea during winter is considerably weaker than in the northern Arabian Sea (Nair et al., 1989; Curry et al., 1992; Ittekot et al., 1992; Antoine et al., 1996). In addition, sediment traps show that PP is still higher in the eastern Arabian Sea during summer under the current climate regime (Nair et al., 1989; Curry et al., 1992; Ittekot et al., 1992).

As an alternative to direct forcing by summer insolation, more complex scenarios can be invoked to explain the apparent relationship between productivity in the Arabian Sea and winter insolation. Webster (1987) and Webster et al., (1998), for instance, proposed that latent heat forcing, rather than direct heat forcing, is the main mechanism that controls the strength of the monsoon. According to this explanation, strong trade winds in the south Indian Ocean, when boreal summer insolation is low, result in enhanced evaporation in the Southern Hemisphere and increased water vapor supply to the Arabian Sea. Condensation of water vapor, therefore, intensifies the monsoon by releasing heat to the convective cells on the Indian continent (Cadet and Reverdin, 1981; Webster, 1987; Clemens and Oglesby, 1992; Clemens et al., 1996). Such a link between an intensified summer monsoon and stronger Indian Ocean trade winds could explain the good match between OC profiles in cores MD900963 in the eastern Maldives and MD88-769 in the Subantarctic Indian Ocean (Fig. 4). This coupling could also be tested by comparing directly the U and Cd records in the same two cores (Fig. 5). Although the records exhibit common maxima during isotope stages 6, 5.4, 5.2, and 4, there are also clear differences such as those between the two Cd records. This suggests that coupling between Cd and U accumulation, and/or the effects of secondary remobilization, are not strictly equivalent at these two locations despite an apparent similar burial of bulk organic matter (Fig. 4).

5. CONCLUSIONS

U, Cd, Mo, OC, and $totC_{37}$ records, representative of the eastern equatorial Arabian Sea over the past 330 kyr, are in phase and dominated by a 23-kyr precessional cycle. Comparison with U, Mo, and Cd concentrations in different environments indicates that the water column never turned completely anoxic in this area. Instead, the redox state of the sediment has fluctuated between oxic and mildly suboxic conditions. Strong positive correlations among organic constituents, authigenic metals, and a number of other proxies keenly suggests that the flux of organic matter reaching the sediment controlled the redox state of the sediment and the accumulation of metals and organic matter over the past 330 kyr. Cd and U enrichments could be due to both mechanisms of precipitation of U and Cd dissolved in porewaters and the direct influx of U and Cd with sinking particles. Both processes are ultimately linked to surface biologic productivity.

The geochemical records in core MD900963 are dominated by precessional forcing due to primary productivity increase in phase with low summer insolation in the Northern Hemisphere. Comparison with other records from the Arabian Sea indicates that periods of increased PP at core MD900963 were synchronous possibly due to mechanisms regulating the winter monsoon winds and/or the southern trade winds. Primary productivity in the Arabian Sea, therefore, seems to have been in phase with summer insolation only in the region directly influenced by coastal upwelling.

REFERENCES

Anderson R. F. (1987) Redox behavior of Uranium in an anoxic marine basin. *Uranium* **3**, 145–164.

Antoine D., André J.-M., and Morel A. (1996) Oceanic primary production 2. Estimation at global scale from satellite (coastal zone color scanner) chlorophyll. *Global Biogeochem. Cy.* **10**, 57–69.

Banse K. and McClain C. R. (1986) Winter blooms of phytoplankton in the Arabian Sea observed by the Coastal Zone Color Scanner. *Mar. Ecol.-Prog. Ser.* **34**, 201–211.

Barnes C. E. and Cochran J. K. (1990) Uranium removal in oceanic sediments and the oceanic U balance. *Earth Planet. Sci. Lett.* **97**, 94–101.

Bassinot F. C. (1993) Analyse paléocéanographique à haute résolution des carbonates pélagiques des Océans Indien et Pacifique en région tropicale. PhD. dissertation, Univ. Aix-Marseille.

Bassinot F. C., Labeyrie L. D., Vincent E., Quidelleur X., Shackleton N. J., and Lancelot Y. (1994a) The astronomical theory of climate and the age of the Brunhes-Matuyama magnetic reversal. *Earth Planet. Sci. Lett.* **126**, 91–108.

Bassinot F. C., Beaufort L., Vincent E., Labeyrie L. D., Rostek F., Muller P. J., Quidelleur X., and Lancelot Y. (1994b) Coarse fraction fluctuations in pelagic carbonate sediments from the tropical Indian Ocean: A 1500-kyr record of carbonate dissolution. *Paleoceanography* **9**, 579–600.

Beaufort L., Lancelot Y., Camberlin P., Cayre O., Vincent E., Bassinot F., and Labeyrie L. (1997) Insolation cycles as a major control of equatorial Indian Ocean primary production. *Science* **278**, 1451–1545.

Beaufort L., Bassinot F., and Vincent E. (1999) Primary production response to orbitally induced variations of the Southern Ocillation in the Equatorial Indian Ocean. In *Reconstructing Ocean History: A Window into the Future* (ed. F. Abrantes and A. C. Mix) pp. 245–272, Kluwer Academic/Plenum Publishers, New York.

Berger A. L. and Loutre M. F. (1991) Insolation values for the climate of the last 10 million years. *Quaternary Sci. Rev.* **10,** 297–317.

Berner R. A. (1981) A new geochemical classification of sedimentary environments. *J. Sediment. Petrol.* **51,** 359–365.

Boyle E. A. (1992) Cadmium and δ^{13}C paleochemical ocean distributions during the stage 2 glacial maximum. *Annu. Rev. Planet. Sci.* **20,** 245–287.

Boyle E. A., Labeyrie L., and Duplessy J. -C. (1995) Calcitic foraminiferal data confirmed by cadmium in aragonitic *Hoeglundina*: Application to the last glacial maximum in the northern Indian Ocean. *Paleoceanography* **10,** 881–900.

Brock J. C., McClain C. R., Luther M. E., and Hay W. W. (1991) The phytoplankton bloom in the northwestern Arabian Sea during the southwest monsoon of 1979. *J. Geophys. Res.* **96,** 20623–20642.

Cadet D. and Reverdin G. (1981) Water vapour transport over the Indian Ocean during summer 1975. *Tellus* **33,** 5476–5487.

Cayre O., Beaufort L., and Vincent E. (1999) Paleoproductivity in the equatorial Indian Ocean for the last 260,000 yrs: A transfer function based on planktonic foraminifera. *Quaternary Sci. Rev.* **18,** 839–857.

Chesner C. A., Rose W. I., Deino A., Drake R., and Westgate J. A. (1991) Eruptive history of earth's largest Quaternary caldera (Toba, Indonesia) clarified. *Geology* **19,** 200–203.

Clemens S. C. and Prell W. L. (1990) Late Pleistocene variability of Arabian Sea summer monsoon winds and continental aridity: Eolian records from lithogenic component of deep-sea sediments. *Paleoceanography* **5,** 109–145.

Clemens S. C. and Oglesby R. J. (1992) Interhemispheric moisture transport in the Indian Ocean summer monsoon: Data-model and model-model Comparisons. *Paleoceanography* **7,** 633–643.

Clemens S. C., Prell W. L., Murray D., Shimmield G., and Weedon G. (1991) Forcing mechanisms of the Indian Ocean monsoon. *Nature* **353,** 720–725.

Clemens S. C., Murray D., and Prell W. L. (1996) Nonstationary phase of the Plio-Pleistocene Asian monsoon. *Science* **274,** 943–948.

Cochran J. K., Carey A. E., Sholkovitz E. R., and Surprenant L. D. (1986) The geochemistry of uranium and thorium in coastal marine sediments and sediment pore waters. *Geochim. Cosmochim. Acta* **50,** 663–680.

Crusius J., Calvert S., Pedersen T., and Sage D. (1996) Rhenium and molybdenum enrichments in sediments as indicators of oxic, suboxic and sulfidic conditions of deposition. *Earth Planet. Sci. Lett.* **145,** 65–78.

Curry W. B., Ostermann D. R., Guptha M. V. S., and Ittekkot V. (1992). Foraminiferal production and monsoonal upwelling in the Arabian Sea: Evidence from sediment traps. In *Upwelling Systems: Evolution Since the Early Miocene* (ed. C. P. Summerhayes, et al.) Geological Society Special Publication **64,** 93–106.

Da Silva A., Young A. C., and Levitus S. (1994) *Atlas of Surface Marine Data 1994, Volume 1: Algorithms and Procedures.* U.S. Department of Commerce.

Emeis K.-C., Anderson D. M., Doose H., Kroon D., and Schulz-Bull D. (1995) Sea-surface temperatures and the history of monsoon upwelling in the northwest Arabian Sea during the last 500,000 years. *Quaternary Res.* **43,** 355–361.

Emerson S. R. and Bender M. (1980) Carbon fluxes at the sediment-water interface of the deep-sea: Calcium carbonate preservation. *J. Mar. Res.* **39,** 139–162.

Emerson S. R. and Huested S. S. (1991) Ocean anoxia and the concentrations of molybdenum and vanadium in seawater. *Mar. Chem.* **34,** 177–196.

Fontugne, M. R. and Duplessy J. C. (1986) Variations in the monsoon regime during the upper Quaternary: Evidence from carbon isotopic record of organic matter in North Indian Ocean sediment cores. *Palaeogeogr. Palaeocl.* **56,** 69–88.

François R., Altabet M. A., Yu E.-F., Sigman D., Bacon M. P., Fank M., Bohrmann G., Bareille G., and Labeyrie L. D. (1997) Contribution of Southern Ocean surface-water stratification to low atmo-

spheric CO_2 concentrations during the last glacial period. *Nature* **389,** 929–935.

Froelich P. N., Klinkhammer G. P., Bender M. L., Luedtke N. A., Heath G. R., Cullen D., and Dauphin P. (1979) Early oxydation of organic matter in pelagic sediments of the eastern equatorial Atlantic: Suboxic diagenesis. *Geochim. Cosmochim. Acta* **43,** 1075–1090.

Haake B., Rixen T., Reemtsma T., Ramaswamy V., and Ittekot V. (1996) Processes determining seasonality and interannual variability of settling particle fluxes to the deep Arabian Sea. In *Particle Flux in the Ocean* (ed. V. Ittekot et al.), pp. 251–270, Wiley & Sons.

Haddad G. A. (1994) Calcium carbonate dissolution patterns at intermediate water depths of the tropical oceans during the Quaternary. Ph.D. dissertation, Rice University, Houston.

Imbrie J. and Imbrie J. Z. (1980) Modeling the climatic response to orbital variations. *Science* **207,** 943–953.

Ittekot V., Haake B., Bartsch M., Nair R. R., and Ramaswamy V. (1992) Organic carbon removal in the sea: The continental connection. In *Upwelling Systems: Evolution Since the Early Miocene* (ed. C.P. Summerhayes et al.), Vol. 64, pp. 167–176. Geol. Soc. Spec. Pub., London.

Kallel N., Labeyrie L. D., Juillet-Leclerc A., and Duplessy J.-C. (1988) A deep hydrological front between intermediate and deep-water masses in the glacial Indian Ocean. *Nature* **333,** 651–655.

Klinkhammer G. P. and Palmer M. R. (1991) Uranium in the oceans: Where it goes and why. *Geochim. Cosmochim. Acta* **55,** 1799–1806.

Knox R. A. (1987) The Indian Ocean: Interaction with the monsoon. In *Monsoons* (ed. J. S. Fein and P. L. Stephens), pp. 365–397, Wiley Interscience, New York.

Kroopnick P. M. (1985) the distribution of ^{13}C of ΣCO_2 in the world oceans. *Deep-Sea Res.* **32,** 57–84.

Kumar N., Anderson R. F., Mortlock R. A., Froelich P. N., Kubik P., Dittrich-Hannen B., and Suter M. (1995) Increased biological productivity and export production in the glacial Southern Ocean. *Nature* **378,** 675–680.

Kutzbach, J. E. and Guetter P. J. (1986) The influence of changing orbital parameters and surface boundary conditions on climate simulations for the last 18,000 years. *J. Atmos. Sci.* **43,** 1726–1759.

Kuwabara J. S., van Geen A., McCorkle D. C., and Bernhard J. M. (1999) Dissolved sulfide distributions in the water column and sediment pore waters of the Santa Barbara basin. *Geochim. Cosmochim. Acta* **63,** 2199–2209.

Lapp B. and Balzer W. (1993) Early diagenesis of trace metals used as an indicator of past productivity changes in coastal sediments. *Geochim. Cosmochim. Acta* **57,** 4639–4652.

Legeleux F., Reyss J.-L., Bonte P., and Organo C. (1994) Concomitant enrichments of uranium, molybdenum and arsenic in suboxic continental margin sediments. *Oceanol. Acta* **17,** 417–429.

Levitus S. and Boyer T. P. (1994a) *World Ocean Atlas 1994 Volume 2: Oxygen.* U.S. Department of Commerce.

Levitus S. and Boyer T. P. (1994b) *World Ocean Atlas 1994 Volume 4: Temperature.* U.S. Department of Commerce.

Levitus S., Burgett R., and Boyer T. P. (1994) *World Ocean Atlas 1994 Volume 3: Salinity.* U.S. Department of Commerce.

Luther M. E., O'Brien J. J., and Prell W. L. (1990) Variability in upwelling fields in the northwestern Indian Ocean 1. Model experiments for the past 18,000 Years. *Paleoceanography* **5,** 433–445.

Madhupratap M., Prasanna Kumar S., Bhattathiri P. M. A., Dileep Kumar M., Raghukumar S., Nair K. K. C., and Ramaiah N. (1996) Mechanism of the biological response to winter cooling in the northeastern Arabian Sea. *Nature* **384,** 549–552.

Mantyla A. W. and Reid J. L. (1995) On the origins of deep and bottom waters of the Indian Ocean. *J. Geophys. Res.* **100,** 2417–2439.

Marlowe I. T., Green J. C., Neal A. C., Brassel S. C., Eglinton G., and Course P. A. (1984) Long chain (n-C_{37}-C_{39}) alkenones in the Prymnesiophyceae. Distribution of alkenones and other lipids and their taxonomic significance. *Brit. Phycol. J.* **19,** 203–216.

McCorkle D. C., Heggie D. T., and Veeh H. H. (1998) Glacial and Holocene stable isotope distributions in the southeastern Indian Ocean. *Paleoceanography* **13,** 20–34.

Murray D. W. and Prell W. L. (1992) Late Pliocene and Pleistocene climatic oscillations and monsoon upwelling recorded in sediments from the Owen Ridge, northwestern Arabian Sea. In *Upwelling*

Systems: Evolution Since the Early Miocene (ed. C.P. Summerhayes et al.), Vol. 64, pp. 301–321. Geol. Soc. Spec. Pub., London.

Nagender N. B., Bau M., Ramalingeswara R. B., and Rao C. M. (1997) Trace and rare earth elemental variation in the Arabian Sea sediments through a transect across the oxygen minimum zone. *Geochim. Cosmochim. Acta* **61**, 2375–2388.

Naidu P. D., Babu C. P., and Rao C. M. (1992) The upwelling record in the sediments of the western continental margin of India. *Deep-Sea Res.* **39**, 715–723.

Naidu P. D., Kumar M. R. R., and Babu V. R. (1999) Time and space variations of monsoonal upwelling along the west and east coast of India. *Cont. Shelf Res.* **19**, 559–572.

Nair R. R., Ittekot V., Manganini S. J., Ramaswamy V., Haake B., Degens E. T., Desai B. N., and Honjo S. (1989) Increased particle flux to the deep ocean related to monsoons. *Nature* **338**, 749–751.

Ninkovich D., Shackleton N. J., Abdel-Monem A. A., Obradovich J. D., and Izett G. (1978) K-Ar age of the late Pleistocene eruption of Toba, north Sumatra. *Nature* **276**, 574–577.

Olson D. B., Hitchcock G. L., Fine R. A., and Warren B. A. (1993) Maintenance of the low-oxygen layer in the central Arabian Sea. *Deep-Sea Res. Pt. II* **40**, 673–685.

Prahl F. G. and Muelhausen L. A. (1989) Lipid biomarkers as geochemical tools for Paleoceanographic study. In *Productivity of the Ocean: Present and Past* (ed. W. H. Berger et al.), pp. 271–289, Wiley & Sons.

Prell W. L. (1984) Monsoonal climate of the Arabian Sea during the late Quaternary: A response to changing solar radiation. In *Milankovitch and Climate, Part 1* (ed. A. L. Berger et al.), pp. 349–366. D. Reidel Pub. Co., Dordrecht.

Prell W. L. and Kutzbach J. E. (1992) Sensitivity of the Indian monsoon to forcing parameters and implications for its evolution. *Nature* **360**, 647–652.

Rao R. R., Molinari R. L., and Festa J. F. (1989) Evolution of the climatological near-surface thermal structure of the tropical Indian Ocean 1. Description of mean monthly mixed layer depth, and sea surface temperature, surface current, and surface meteorological fields. *J. Geophys. Res.* **94**, 10801–10815.

Reichart G. J., den Dulk M., Visser H. J., van der Weijden C. H., and Zachariasse W. J. (1997) A 225 kyr record of dust supply, paleoproductivity and the oxygen minimum zone from the Murray Ridge (northern Arabian Sea). *Palaeogeogr. Palaeocl.* **134**, 149–169.

Reichart G. J., Lourens L. J., and Zachariasse W. J. (1998) Temporal variability in the northern Arabian Sea Oxygen Minimum Zone (OMZ) during the last 225,000 years. *Paleoceanography* **13**, 607–621.

Rosell-Melé A., Bard E., Emeis K. C., Grimalt J. O., Müller P., Schneider R. R., Blanz T., Bouloubassi I., Epstein B., Fahl K., Fluegge A., Freeman K., Goni M., Güntner U., Hartz D., Hellebust S., Herbert T., Ikehara M., Ishiwatari R., Kawamura K., Kenig F., de Leeuw J., Lehman S., Mejanelle L., Ohkouchi N., Pancost R. D., Pelejero C., Prahl F., Quinn J., Rontani J. F., Rostek F., Rüllkotter J., Sachs J., Sawada K., Schulz-Bull D., Sikes E., Sonzogni C., Ternois Y., Versteegh G., Volkman J., and Wakeham S. (2001) Precision of the current methods to measure the alkenone proxy UK37′ and absolute abundance in sediments: Results of an interlaboratory comparison study. *Geochem. Geophys. Geosys.* **2**, 1–28.

Rosenthal Y., Lam P., Boyle E. A., and Thomson J. (1995a) Authigenic cadmium enrichments in suboxic sediments: Precipitation and post-depositional mobility. *Earth Planet. Sci. Lett.* **132**, 99–111.

Rosenthal Y., Boyle E. A., Labeyrie L., and Oppo D. (1995b) Glacial enrichments of authigenic Cd and U in Subantarctic sediments: A climatic control on the elements' organic budget? *Paleoceanography* **10**, 395–413.

Rosenthal Y., Boyle E. A., and Labeyrie L. (1997) Last glacial maximum paleochemistry and deepwater circulation in the Southern Ocean: Evidence from foraminiferal cadmium. *Paleoceanography* **12**, 787–796.

Rostek F., Bard E., Beaufort L., Sonzogni C., and Ganssen G. (1997) Sea surface temperature and productivity records for the past 240 kyr in the Arabian Sea. *Deep-Sea Res. Pt. II* **44**, 1461–1480.

Sarkar A., Bhattacharya S. K., and Sarin M. M. (1993) Geochemical evidence for anoxic deep water in the Arabian Sea during the last glaciation. *Geochim. Cosmochim. Acta* **57**, 1009–1016.

Sastry J. S. and D'Souza R. S. (1972) Upwelling and upward mixing in the Arabian Sea. *Indian J. Mar. Sci.* **1**, 17–27.

Schubert C. J., Villanueva J., Calvert S. E., Cowie G. L., von Rad U., Schulz H., Berner U., and Erlenkeusser H. (1998) Stable phytoplankton community structure in the Arabian Sea over the past 200,000 years. *Nature* **394**, 563–566.

Schulte S., Rostek F., Bard E., Rullkötter J., Marchal O. (1999) Variations of oxygen-minimum and primary productivity recorded in sediments of the Arabian Sea. *Earth Planet. Sci. Lett.* **173**, 205–221.

Schulz H., von Rad U., and Erlenkeuser H. (1998) Correlation between Arabian Sea and Greenland climate oscillations of the past 110,000 years. *Nature* **393**, 54–57.

Sharma G. S. (1978) Upwelling off the southwestern coast of India. *Indian J. Mar. Sci.* **7**, 209–218.

Shimmield G. B. (1992) Can sediment geochemistry record changes in coastal upwelling palaeoproductivity? Evidence from northwest Africa and the Arabian Sea. In *Upwelling Systems: Evolution Since the Early Miocene* (ed. C.P. Summerhayes et al.), Vol. 64, pp. 29–46. Geol. Soc. Spec. Pub., London.

Shimmield G. B. and Price N. B. (1986) The behaviour of molybnenum and manganese during early sediment diagenesis—Offshore Baja California, Mexico. *Mar. Chem.* **19**, 216–280.

Sirocko F. (1995) Abrupt change in monsoonal climate: Evidence from the geochemical composition of Arabian sea sediments. Habilitation thesis, University of Kiel.

Sirocko F., Sarnthein M., Erlenkeuser H., Lange H., Arnold M., and Duplessy J.-C. (1993) Century-scale events in monsoonal climate over the past 24,000 years. *Nature* **364**, 322–324.

Sonzogni C., Bard E., Rostek F., Lafont R., Rosell-Mele A., and Eglinton G. (1997) Core-top calibration of the alkenone index vs. sea surface temperature in the Indian Ocean. *Deep-Sea Res. Pt. II* **44**, 1445–1460.

Stuiver M., Quay P. D., and Ostlund H. G. (1983) Abyssal water carbon-14 distribution and the age of the world oceans. *Science* **219**, 849–851.

Taylor S. R. and McLennan S. M. (1985) *The Continental Crust: Its Composition and Evolution.* Blackwells.

Tchernia P. (1980) *Descriptive Regional Oceanography*, pp. 165–208, Pergamon Press.

Thomson J., Jarvis I., Green D. R. H., Green D. A., and Clayton T. (1998) Mobility and immobility of redox-sensitive elements in deep-sea turbidites during shallow burial. *Geochim. Cosmochim. Acta* **62**, 643–656.

van Geen A., McCorkle D. C., and Klinkhammer G. P. (1995) Sensitivity of the phosphate-cadmium-carbon isotope relation in the ocean to cadmium removal by suboxic sediments. *Paleoceanography* **10**, 159–169.

Verardo D. J., Froelich P. N., and McIntyre A. (1990) Determination of organic carbon and nitrogen in marine sediments using the Carlo Erba NA-1500 Analyser. *Deep-Sea Res.* **37**, 157–165.

Villanueva J., Grimalt J. O., Labeyrie L., Cortijo E., Vidal L., and Turon J.-L. (1998) Precessional forcing of productivity in the North Atlantic Ocean. *Paleoceanography* **13**, 561–571.

Volkman J. K., Eglinton G., Corner E. D. S., and Sargent J. R. (1980a) Novel unsaturated straight-chain C_{37}-C_{39} methyl and ethyl ketones in marine sediments and a coccolithophore *Emiliania huxleyi*. In *Advances in Organic Geochemistry* (ed. A. G. Douglas and J. R. Maxwell), pp. 219–227, Pergamon Press.

Volkman J. K., Eglinton G., Corner E. D. S., and Forsberg T. E. V. (1980b) Long-chain alkenes and alkenones in the marine coccolithophorid *Emiliania huxleyi. Phytochemistry* **19**, 2619–2622.

Wallace H. E., Thomson J., Wilson T. R. S., Weaver P. P. E., Higgs N. C., and Hydes D. J. (1988) Active diagenetic formation of metal-rich layers in N.E. Atlantic sediments. *Geochim. Cosmochim. Acta* **52**, 1557–1569.

Webster P. J. (1987) The elementary monsoon. In *Monsoons* (ed. J. S. Fein J.S. and P.L. Stephens), pp. 3–32, Wiley-Interscience.

Webster P. J., Magaña V. O., Palmer T. N., Shukla J., Tomas R. A., Yanai M., and Yasunari T. (1998) Monsoons: Processes, predictability, and the prospects for prediction. *J. Geophys. Res.* **103**, 14451–14510.

Westgate J. A., Shane P. A. R., Pearce N. J. G., Perkins W. T., Korisettar R., Chesner C. A., Williams M. A. J., and Acharyya S. K.

(1998) All Toba tephra occurrences across Peninsular India belong to the 75 kyr B.P. *Eruption. Quat. Res.* **50,** 107–112.

Willamowski C., Hamelin B., Bard E. (2001) Paleoventilation conditions in the equatorial Indian Ocean between 300 and 500 ka BP. *EUG XI, J. of Conf. Abstracts.* **6,** 113.

Wilson T. R. S., Thomson J., Colley S., Hydes D. J., and Higgs N. C. (1985) Early organic diagenesis: The significance of progressive subsurface oxydation fronts in pelagic sediments. *Geochim. Cosmochim. Acta* **49,** 811–822.

Wyrtki K. (1973) Physical oceanography of the Indian Ocean. In *Biology of the Indian Ocean* (ed. S. Zeitschel), Vol. 3, pp. 18–36. Springer, Berlin.

Zheng, Y., Anderson R. F., van Geen A., and Kuwabara J. S. (2000) Controls of authigenic Mo formation in marine sediment: Linkage to pore water sulfide. *Geochim. Cosmochim. Acta* **64,** 4165–4178.

Zheng, Y., Anderson R. F., van Geen A., and Fleisher M. (2001a) Remobilization of authigenic uranium from marine sediments by bioturbation, submitted to *Geochim. Cosmochim. Acta* December 2000.

Zheng, Y., Anderson R. F., van Geen A., and Fleisher M. (2001b) Preservation of particulate non-lithogenic sediments in marine sediments. *Geochim. Cosmochim. Acta*, in press.

Zheng, Y., Weinman B., Cronin T., Fleisher M., and Anderson R. F. (2001c) A rapid procedure for thorium, uranium, cadmium and molybdenum in small sediment samples by inductively coupled plasma-mass spectrometer and application in Chesapeake Bay, submitted to *Appl. Geochem.*